Carbonates and Evaporites (2023) 38:72
https://doi.org/10.1007/s13146-023-00897-3

ORIGINAL ARTICLE

Characterization of the Govanda Formation limestones: chemostratigraphy and tectonic setting of the last marine carbonate rocks in the Arabia–Eurasia suture zone, NW Zagros fold-thrust belt

Zhin S. Abdulrehman[1] · Ahmed M. Aqrawi[1] · Renas I. Koshnaw[2]

Accepted: 14 September 2023 / Published online: 5 October 2023

Abstract

Three stratigraphic sections were sampled to demystify the geochemical properties of the shallow marine Govanda Formation, located in the Arabia–Eurasia suture zone at ~1500 m above sea level. This study examined the geochemistry of major, trace, rare earth elements (REE) and the petrography of carbonate rocks of the lower–middle Miocene Govanda Formation. Microfacies analysis shows that packstone and wackestone dominate the ticker western section, whereas the eastern sections contain grainstone and clastic units. The carbonates were deposited in shallow marine reef-fore-reef environments unaffected by diagenetic alterations. The limestone beds have a consistent seawater-like REE pattern, slightly negative Ce anomalies (Ce/Ce* = 0.79 in massive limestone–MSL and = 0.89 in marly limestone–ML), relatively positive Eu anomalies (Eu/Eu* = 1.18 in MSL and = 1.14 in ML), and moderately high Y/Ho ratios (37.69 $n = 29$). The REE + Y pattern of samples mainly retains its original characters, but the variations in the total rare earth element (ΣREE) content are detected, which could reflect minor detrital material inputs. Authigenic U, negative Ce anomalies, and trace element ratio indices such as V/Cr, U/Th, Ni/Co, and V/(V + Ni) indicate suboxic–anoxic deposition condition. A positive correlation of Al_2O_3% contents with Fe_2O_3% links the carbonate units of the Govanda Formation to marine limestones. The Rb–Sr-Ba ternary diagram, and Sr/Ba vs. Sr/Rb, Al_2O_3% vs. Fe_2O_3%, and Ce/Ce* vs. Sm/Yb bivariate analyses imply that the studied limestones originated in a passive margin tectonic setting.

Keywords Arabia–Eurasia suture zone · Chemostratigraphy · Govanda Formation · Rare earth elements (REE) · Zagros fold–thrust belt

Introduction

After the Arabia–Eurasia collision during the Oligocene and before the regional uplift of the Arabia–Eurasia suture zone during the late Miocene, a marine seaway connected the Mediterranean Sea and the Indian Ocean in the early–middle Miocene period (Hempton 1987; Allen and Armstrong 2008; Zadeh et al. 2017; Koshnaw et al. 2019, 2021; Mohammadkhani et al. 2022). During the early and middle Miocene, a relatively warm climate, known as the Middle Miocene Climatic Optimum (MMCO), was characterized by a high sea level (Zachos et al. 2001; Miller et al. 2020). The preserved dispatched shallow marine lower-middle Miocene carbonate rocks in the Arabia–Eurasia suture zone in the Kurdistan region of Iraq represent a record of this post-collisional marine incursion. The marine limestone beds of the Govanda Formation were deposited on the nonmarine clastic beds of the Suwais Group and are stratigraphically followed by nonmarine clastic beds of the Merga Group, suggesting a period of marine water incursion. These three rock units collectively, known as the Red Beds Series (RBS), were deposited in an intermontane basin setting in the Arabia–Eurasia suture zone after the collision (van Bellen et al. 1959; Jassim et al. 2006; Koshnaw et al. 2021).

The rare earth element and Y (REE + Y) signature of carbonates has been widely exploited in recent decades to reconstruct the history of deep-marine paleoenvironment

✉ Zhin S. Abdulrehman
zhin.abdulrehman@gmail.com

[1] Earth Sciences and Petroleum Department, College of Science, Salahaddin University–Erbil, Erbil, Kurdistan Region, Iraq

[2] Department of Structural Geology and Geodynamics, Geoscience Center, University of Gottingen, Gottingen, Germany

(Piper 1974; Elderfield et al. 1990; Armstrong-Altrin et al. 2003; Madhavaraju et al. 2010; Nagarajan et al. 2011; Özyurt et al. 2020). REEs + Y have systematic changes in the chemical properties of the marine system due to the progressive filling of the outer shell. This causes different fractionations of REEs + Y in natural systems. Except for europium (Eu^{+2}, Eu^{+3}) and cerium (Ce^{+3}, Ce^{+4}), all REEs have a trivalent character which is redox-sensitive elements, and they show distinct geochemical behavior compared to other Lanthanides (Caetano-Filho et al. 2018; Özyurt et al. 2020). Through these geochemical characterizations, carbonate sedimentologists can reconstruct ancient environmental conditions. The carbonate succession of the Govanda Formation is well defined in terms of its stratigraphical and sedimentological characteristics (Smail 2015; Abdula et al. 2018). Sediments are platform carbonates which are represented by microfacies analysis indicating a transition towards a quieter lagoonal/reefal environment upward in the sequence and the compaction is the main diagenetic process that occurs between the grains that are returned to the close of the formation to the thrust zone and plate boundary (Smail 2015). Although there were several studies that dealt with Govanda Formation in terms of sedimentology, stratigraphy, and paleoecology, there has not been an attempt to investigate Bulk-rock geochemistry and elemental variation that provide proxies for paleo-redox conditions controls on their geochemistry. Consequently, this study focuses on the limestone strata outcropping in the Soran area in the northwestern Zagros fold–thrust belt within the intermontane Red Bed basin (NE Iraq) and presents a petrographic analysis coupled with REE + Y characterization of the limestone succession. The main purpose of the current study is (1) to determine ancient seawater composition using marine carbonates of intermountain basin NW Zagros thrust zone and affected by detrital materials; (2) to define the redox conditions and discuss the pale-oceanographic proxies for discrimination of depositional tectonic settings and paleoenvironments of the limestones and (3) to discuss the role of potential diagenetic influence on REE signals of ancient carbonates. The geochemical results were substantiated by field and petrographic studies and an extensive literature review.

Geological setting

From southeast Turkey and across the Kurdistan area of Iraq to southwestern Iran, the NW–SE trending Zagros orogenic belt extends for around 2000 km. It was produced during the Cenozoic Arabia–Eurasia convergence. During the Late Cretaceous (Berriasian–Maastrichtian), ophiolitic terranes were obducted onto the Arabian plate, leading to the Paleogene flexural subsidence and marine clastic input into the developing proto-Zagros foreland basin. Following the Arabia–Eurasia collision, the Zagros orogenic belt expanded forelandward via shortening throughout the Neogene, resulting in clastic material input into the Neogene Zagros foreland basin (Alavi, 2004; Jassim and Goff, 2006; Koshnaw et al. 2020).

The RBS basin, which was developed at the suture zone of Arabia–Eurasia after the Oligocene, was accumulated in a narrow depozone on the plate boundary in a strongly subsiding intermontane basin (Jassim and Goff,

2006; Koshnaw et al. 2021). According to van Bellen et al. (1959), the RBS is subdivided into the lower Suwais Red Beds, the middle Govanda Limestone, and the upper Merga Red Beds. The Govanda Formation features a series of patchy reef bodies along the NW Zagros fold–thrust belt.

According to Buday (1980), the Govanda Formation consists of a shallow marine reef-fore-reef environment and is influenced by sediment supply by nearby paleo highs. The lower contact of the Govanda Formation is unconformable with the Suwais Group. The upper contact is gradational and conformable, gradually transitioning into the red shales and sandstones of the Merga Group (van Bellen et al. 1959; Buday 1980). Along the Arabia–Eurasia suture zone, the RBS rock units are thrusted onto by allochthonous rock units, Naopurdan and Walash. Naopurdan consists of fly-ash sediments and nummulitic limestone beds, whereas the Walash Group consists of igneous rocks (basalt and tuff), sandstone, shale, limestone, and radiolarite (Jassim and Goff 2006; Hassan 2012). The study area in the northeast of Erbil city in the Kurdistan region of Iraq includes three exposed sections with a variance thickness along-strike of ~ 144 m, 60 m, and 23 m, respectively. The first section is Sherwan Mazin section is in the northwestern extremity of the study area (lat. 36° 59′ 7″ N and long. 44° 12′ 18″ E). This stratigraphic secession and thickness changed toward the second (Hababiyan) section (lat. 36° 45′ 7.9″ N and long. 44° 28′ 52.5″ E). To the southeast, the Govanda Formation's thickness decreases further at the Smelan section (lat. 36° 40′ 2.3″ N and long. 44° 42′ 34.8″ E). All three sections are exposed in road-cut outcrops along the Arabia–Eurasia suture zone in the NW Zagros fault-thrust belt (Figs. 1 and 2).

Methods

For this study, 29 samples were collected from three sections to establish the petrographic and geochemical variations of the Govanda Formation. Thin sections have been prepared using the standard methods of thin section preparation and followed Dunham's method for the classification of the studied carbonates. To eliminate any contamination, the selected samples were washed with distilled water. They were then air-dried and finely ground in a tungsten carbide mortar. For further refinement, the ground samples were sieved through

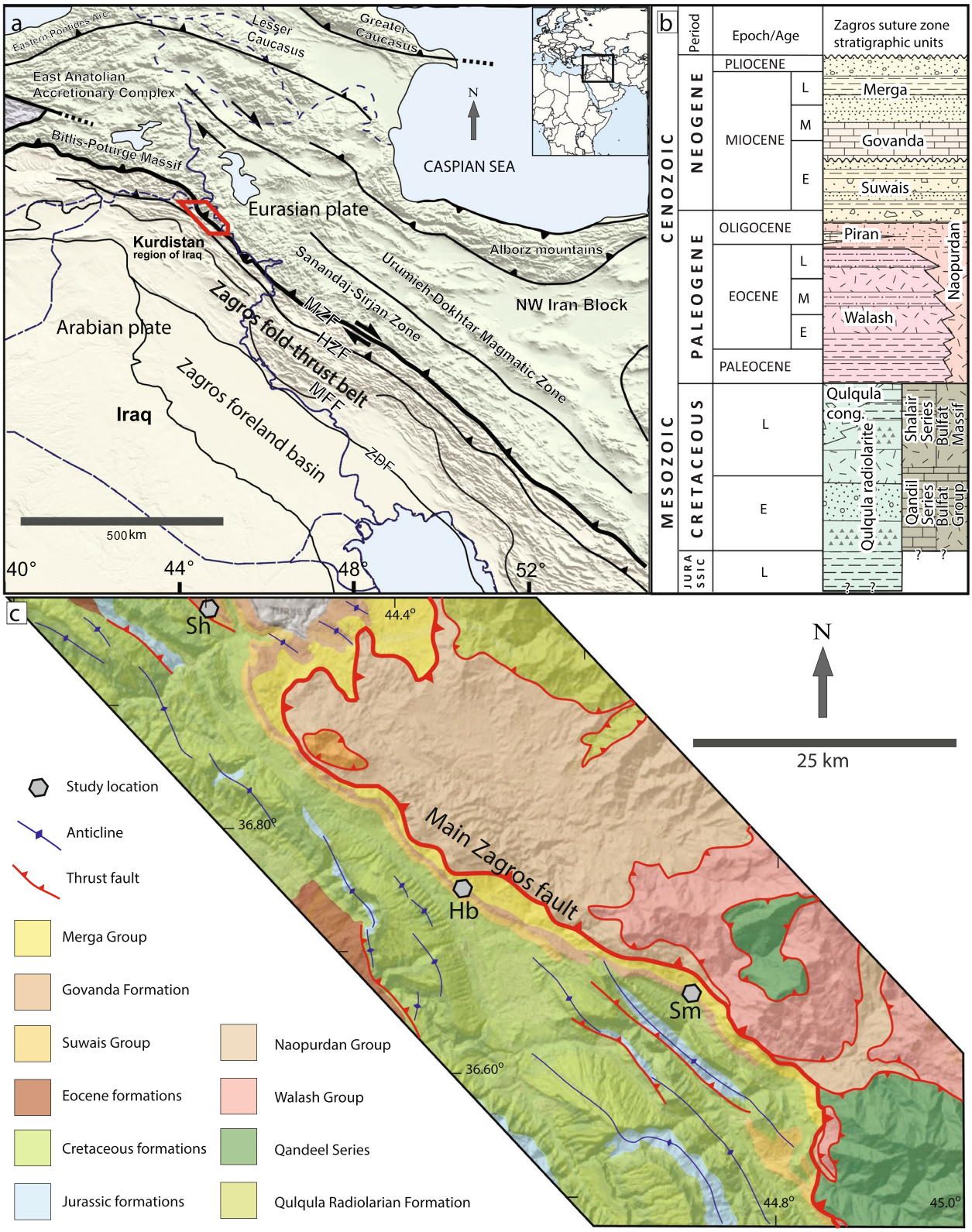

Fig. 1 **a** Regional tectonic map showing location of the study area the Arabia–Eurasia suture zone; **b** Generalized stratigraphic column depicting major rock units in the study area; **c** Geological map of the study area indicating locations of the studied sections in this study (*Sh* Sherwan Mazen, *Hb* Hababiyan, and *Se* Semelan) and geographic distribution of the Govanda Formation. Figures modified after Sissakian and Foad (2014) and Koshnaw et al. (2021)

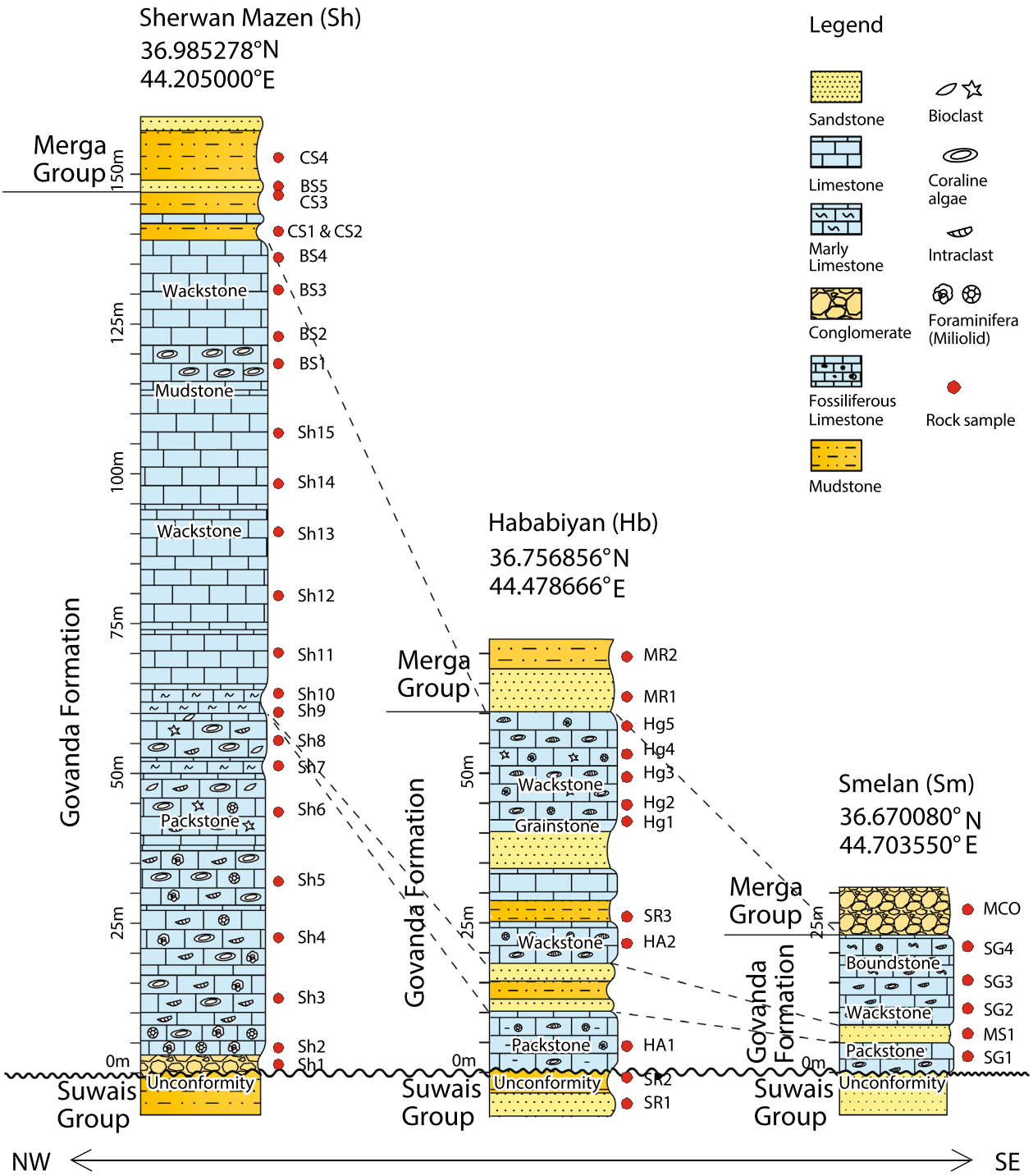

Fig. 2 Stratigraphic sections representing the Govanda Formation in the study area show notable thickness change from northwest to southeast

a 200 ASTM mesh. X-ray fluorescence (XRF) was utilized with a spectrometer to conduct a chemical analysis of major oxides, including Al_2O_3, Fe_2O_3, TiO_2, CaO, MgO, MnO, Na_2O, K_2O, and P_2O_5. One gram of sample was heated to 1000 °C in porcelain crucibles for two hours to measure the loss on ignition (LOI). Inductively coupled plasma-mass spectrometry (ICP-MS) was used to analyze the content of trace elements (Ba, Rb, Cs, Sr, Th, U, Y, Zr, Hf, Nb, Sc, V, Cr, Co, Ni, Cu, and Zn) and rare earth elements (La, Ce, Pr, Nd, Sm, Eu, Gd, Tb, Dy, Er, Ho, Tm, Yb and Lu) after four acid digestion (ME-MS81d and ME-4ACD81 codes). The abovementioned geochemical analyses were performed at

the ALS International Laboratory in Spain. To ensure analytical accuracy and precision, which ranged from 0 to 9.3% and 2 to 8.8%, respectively, the internationally acknowledged standard materials OREAS102a and MRGeo08 were used as references. The Post-Archean Australian Shale (PASS) values given by Taylor and McLennan (1985) were used to prepare REE normalized diagrams.

Results

Petrography

The middle Miocene carbonates of the Govanda Formation are petrographically described according to Dunham's carbonate classification (1962). The petrographic analysis reveals that the carbonate succession has five major microfacies in all studied stratigraphic sections. Benthic (Miliolida) foraminiferal Packstone microfacies (MF-1) is dominated by shallow water benthic foraminiferal packstone with rare wackestone layers. It has a mud-supported texture with some bioclasts in the micritic matrix and the occurrence of calcite

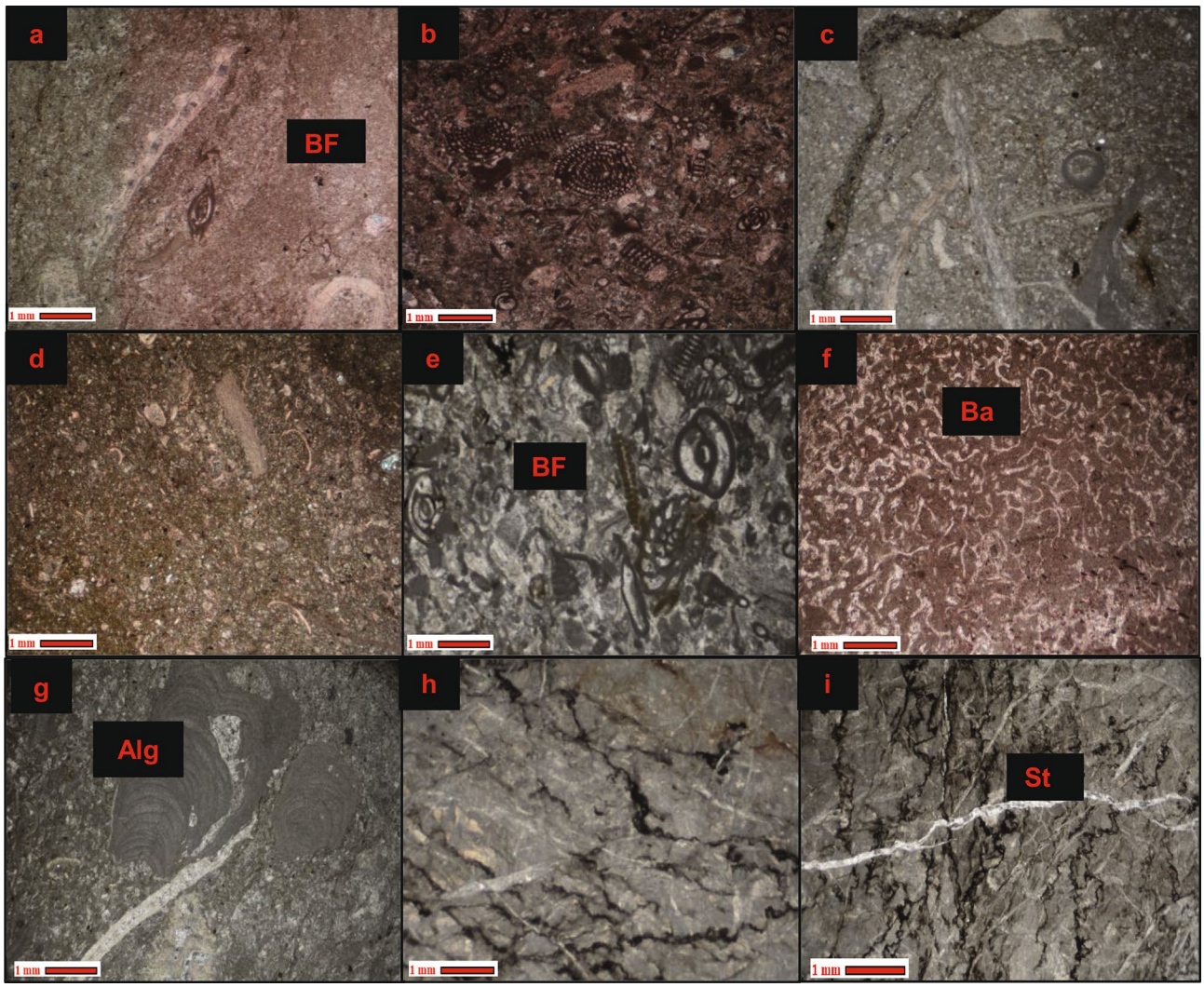

Fig. 3 Thin section views of representative microfacies found in the Govanda Formation; **a**, **b** Benthic (Miliolida) Packstone microfacies (MF-1), samples Sh8 &BS4, cp. **c**, **d** Wackestone microfacies (MF-2), samples Sh15, pp. & Sh9, cp. **e** Foraminiferal Grainstone microfacies (MF-3), sample BS3, pp. **f**, **g** Red algae Boundstone microfacies (MF-4), samples SG3, cp. & Hg2, pp. **h**, **i** Mudstone microfacies (MF-5), sample Sh13, pp., **Bf** Benthic foraminifera, **Ba** Bafflestone, **St** sutured stylolite, **Alg** laminated coralline algae, (*cp* crossed polarizers, *pp* plane polarized)

cementation (Fig. 3a, b). Foraminiferal Wackestone microfacies (MF-2), Most of the grains are composed of skeletal grains like Miliolida, algae, and Alveolinids, and most of the non-skeletal grains are intraclasts in the micritized matrix (Fig. 3c, d). Foraminiferal Grainstone microfacies (MF-3) is mainly composed of fossils of miliolida, alveolinoids, and different kinds of bioclast as well as extra clasts, embedded within sparry calcite groundmass (Fig. 3e). Red algae boundstone (MF-4), The main components this microfacies are encrusted and bound with the other components, and micrite is red coralline algae sheet-like and lamellar skeletons; the predominant faunal association of these facies is coralline red algae, coral, and some foraminiferal-like milliolids (Fig. 3f, g). Lime Mudstone microfacies (MF-5) display a color range from dark gray to dark brown and contain detrital material like clay, silt, and sand. These facies contain a high content of micrite and a smaller number of grains, like some bioclasts with sutured seam stylolite, an irregular type with peaks of low amplitude, in metamorphosed lime mudstone is especially restricted at the upper part of Sherwan Mazin section (Fig. 3h, i). Foraminiferal Wackestone microfacies are primarily found in the middle parts of all studied sections.

Elemental geochemistry

Major and trace elements

Depending on the variation in the content of Al_2O_3, SiO_2 vs. CaO oxides in the studied carbonate samples, which are the sources of different phases (clay and carbonate content), the samples are classified into massive limestones (MSL) and marly limestones (ML) (Fig. 4). The massive limestone is characterized by high purity, approaching the composition of standard calcite (56.03% CaO + 43.97% CO_2; Haldar 2000); it consists of 52.40–55.10% CaO (53.87% av.), 40.80–43.50% LOI (42.41% av.), and 3.1% impurities including SiO_2 (2.18%), Al_2O_3 (0.52%), Fe_2O_{3t} (0.40%), and traces of other oxides (Table 1). The marly limestone is less pure than the massive limestone but still can be considered semi-pure because it also contains relatively high amounts of CaO (42.90–52.90, 47.28% av.),

LOI (34.60–42.20, 38.22% av.), and 14.5% impurities dominated by SiO_2 (9.65%), Al_2O_3 (2.03%), Fe_2O_{3t} (1.08%),

and traces of other oxides (Table 1). The geochemical compositions reveal that the average content of the $CaCO_3$ in ML is lower than in MSL (83.04% and 95.80%, respectively; Table 3). CaO has a negative correlation with SiO_2, Al_2O_3, Fe_2O_{3t}, and P_2O_5 ($r = -0.750$, -0.76, -0.53, and 0.012 in MSL; $r = -0.98$, -0.93, -0.89, and -0.64 in ML, respectively; $n = 29$; Fig. 5) indicating that the source of most major elements is not calcite but rather the impurities in these limestones such as clays, ferruginous material and detrital silica-bearing minerals such as quartz (Lokesh 2015)

Madhavaraju et al. 2016). In addition, CaO% content is significantly higher than the PAAS (Post-Archean Australian Shale)-normalization values of the major elements (Table 1).

Trace element contents (Table 2) were normalized using PAAS values (Taylor and McLennan 1985) and are plotted in Fig. 6. Within the large-ion lithophile elements (LILE) (Rb, Cs, Sr, Ba), Rb, Cs, and Ba are highly depleted compared to the PAAS in both MSL and ML. Sr content within these limestones is higher than the PAAS value (200 ppm; Taylor and McLennan 1985) (Fig. 6; Table 2). An average PAAS normalized of ferromagnesian (Transitional) trace

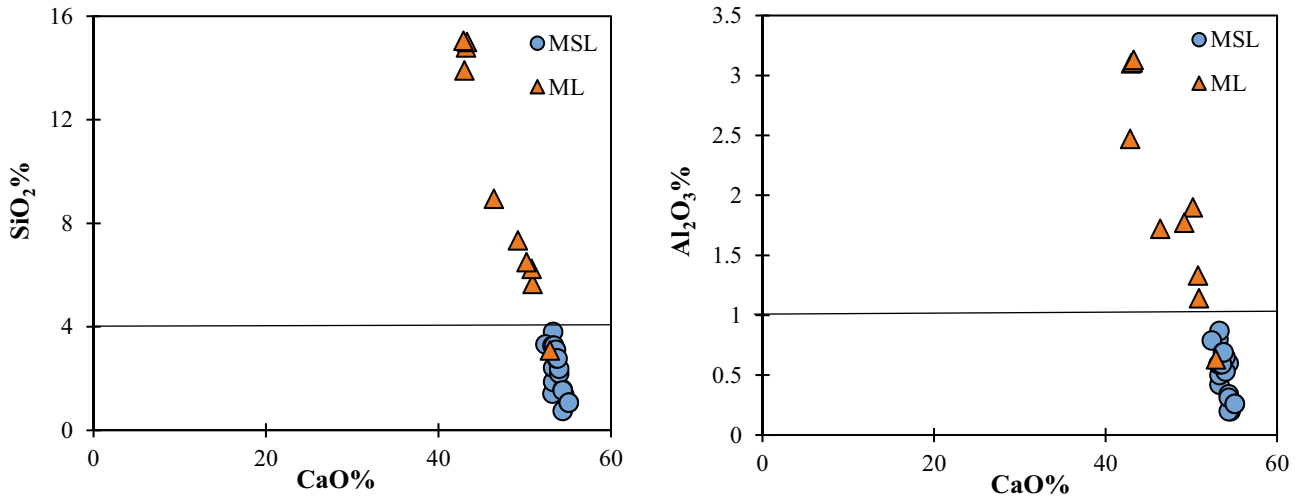

Fig. 4 Bivariation of CaO% vs. Al_2O_3% and CaO% vs. SiO_2% oxides separated the carbonate samples of the studied area into two types: massive limestone (MSL < 4% SiO_2, < 1% Al_2O_3) and marly limestone (ML > 4% SiO_2, > 1% Al_2O_3)

Table 1 Major oxides contents (wt%) of the carbonates of the Govanda Formation, Northeastern Iraq

Rocks	S.No	SiO_2	Al_2O_3	Fe_2O_3	CaO	MgO	Na_2O	K_2O	TiO_2	MnO	P_2O_5	LOI	Total
Massive Limestone (MSL)	Sh2	1.38	0.20	0.20	54.60	1.20	0.04	0.01	0.01	0.03	0.07	43.10	100.84
	Sh3	1.40	0.60	0.60	54.40	1.50	0.06	0.04	0.01	0.02	0.07	42.10	100.80
	Sh4	1.42	0.80	0.80	53.20	1.80	0.07	0.06	0.01	0.03	0.07	42.10	100.36
	Sh8	1.88	0.42	0.29	53.30	1.02	0.05	0.08	0.02	0.01	0.04	42.80	99.91
	Sh11	0.75	0.20	0.15	54.40	1.32	0.05	0.03	0.01	0.01	0.05	43.50	100.47
	Sh13	1.58	0.34	0.19	54.40	0.88	0.04	0.07	0.02	0.01	0.07	43.20	100.80
	Sh14	2.42	0.50	0.28	53.30	1.80	0.06	0.06	0.03	0.01	0.05	42.80	101.31
	BS2	3.81	0.87	0.41	53.30	0.89	0.04	0.19	0.04	0.02	0.04	41.70	101.31
	BS3	2.20	0.65	0.30	54.00	0.69	0.04	0.13	0.03	0.04	0.03	42.50	100.61
	BS3a	2.38	0.53	0.19	54.00	0.68	0.03	0.13	0.03	0.02	0.03	42.50	100.52
	HG1	1.54	0.31	0.57	54.40	0.97	0.05	0.01	0.01	0.01	0.10	42.80	100.77
	HG2	3.32	0.79	0.52	52.40	1.14	0.07	0.15	0.04	0.01	0.06	41.80	100.30
	HG3	3.27	0.59	0.59	53.20	1.26	0.08	0.02	0.04	0.05	0.04	41.70	100.84
	HG4	3.27	0.59	0.59	53.40	1.28	0.08	0.02	0.04	0.06	0.04	41.70	101.07
	HG5	3.11	0.59	0.55	53.60	2.10	0.08	0.02	0.04	0.06	0.04	40.80	100.99
	SG1	2.78	0.69	0.49	53.70	1.16	0.07	0.12	0.03	0.01	0.06	42.20	101.31
	SG2	2.78	0.69	0.49	53.80	1.17	0.08	0.12	0.03	0.01	0.06	42.10	101.33
	SG3	1.07	0.26	0.21	55.10	0.56	0.04	0.06	0.01	0.02	0.03	43.10	100.46
	SG4	1.07	0.26	0.21	55.10	0.57	0.04	0.06	0.01	0.02	0.03	43.30	100.67
	Average	2.18	0.52	0.40	53.87	1.16	0.06	0.07	0.02	0.02	0.05	42.41	100.77
Marly Limestone (ML)	Sh5	13.90	3.10	1.41	43.00	1.14	0.27	0.79	0.18	0.03	0.08	35.60	99.50
	Sh6	14.80	3.11	1.39	43.20	1.16	0.26	0.78	0.18	0.02	0.08	34.60	99.58
	Sh7	15.00	3.13	1.38	43.30	1.18	0.25	0.78	0.18	0.02	0.08	35.60	100.90
	Sh9	8.95	1.72	1.18	46.40	2.58	0.14	0.37	0.09	0.01	0.10	39.10	100.64
	Sh10	15.05	2.47	2.04	42.90	1.72	0.09	0.46	0.11	0.02	0.08	36.00	100.94
	Sh12	3.09	0.63	0.26	52.90	1.10	0.05	0.11	0.04	0.01	0.06	42.20	100.45
	Sh15	5.66	1.14	0.40	50.90	1.07	0.13	0.26	0.07	0.01	0.02	40.60	100.26
	BS1	6.24	1.33	0.62	50.80	1.20	0.05	0.27	0.05	0.03	0.05	40.30	100.94
	HA1	6.50	1.90	1.10	50.20	1.40	0.17	0.35	0.09	0.02	0.07	39.10	100.90
	HA2	7.34	1.77	1.02	49.20	1.32	0.17	0.35	0.09	0.02	0.07	39.10	100.45
	Average	9.65	2.03	1.08	47.28	1.39	0.16	0.45	0.11	0.02	0.07	38.22	100.46
	PAAS	62.40	18.78	7.18	1.29	2.19	1.19	3.68	0.99	0.11	0.16	6.00	103.97

elements (Co, Ni, Cr, and V) showing moderate depletion, except Cr, which shows enrichment in some samples. Within all the high-field strength elements (HFSE) of ML and MSL samples (Zr, Y, Nb, Hf, Th, and U), U shows enrichment in some samples, and others are moderate to highly depleted compared to PAAS (Fig. 6).

Rare earth elements

ΣREE content shows significant variation among the limestone types (average ML = 20.20 ppm and MSL = 7.02 ppm; Table 3). This indicates that the ML is enriched ~ 3 times in REEs relative to MSL, related to the impurities in these limestones. The low ΣREE in these limestones can also be linked to the conditions under which they have been deposited since the marine environments contain minor amounts of detrital constituents and heavy minerals (Piper 1974). REE concentrations in massive and marly limestones are normalized to PAAS values (Taylor and McLennan 1985) in Fig. 6. These limestones are exhibited: (1) seawater-like REE pattern with depletion of light rare earth elements (LREE) relative to heavy rare earth elements (HREE) (av. $(La/Yb)n = 0.64$, 0.71 and $(Nd/Yb)n = 0.64$, 0.76 in MSL and ML, respectively; Table 4); (2) moderate negative Ce* and positive La/La* anomalies (av. 0.79, 1.66, and 0.89, 1.08 in MSL and ML, respectively; Table 4); (3) distinctive positive Gd/Gd* and Eu/Eu* anomalies (av. = 1.34, 1.18 and 0.94, 1.14 in MSL and ML, respectively; Table 4); (4) moderately high Y/Ho ratio (av. Y/Ho = 41.5, 30.4 in MSL and ML, respectively; Table 4).

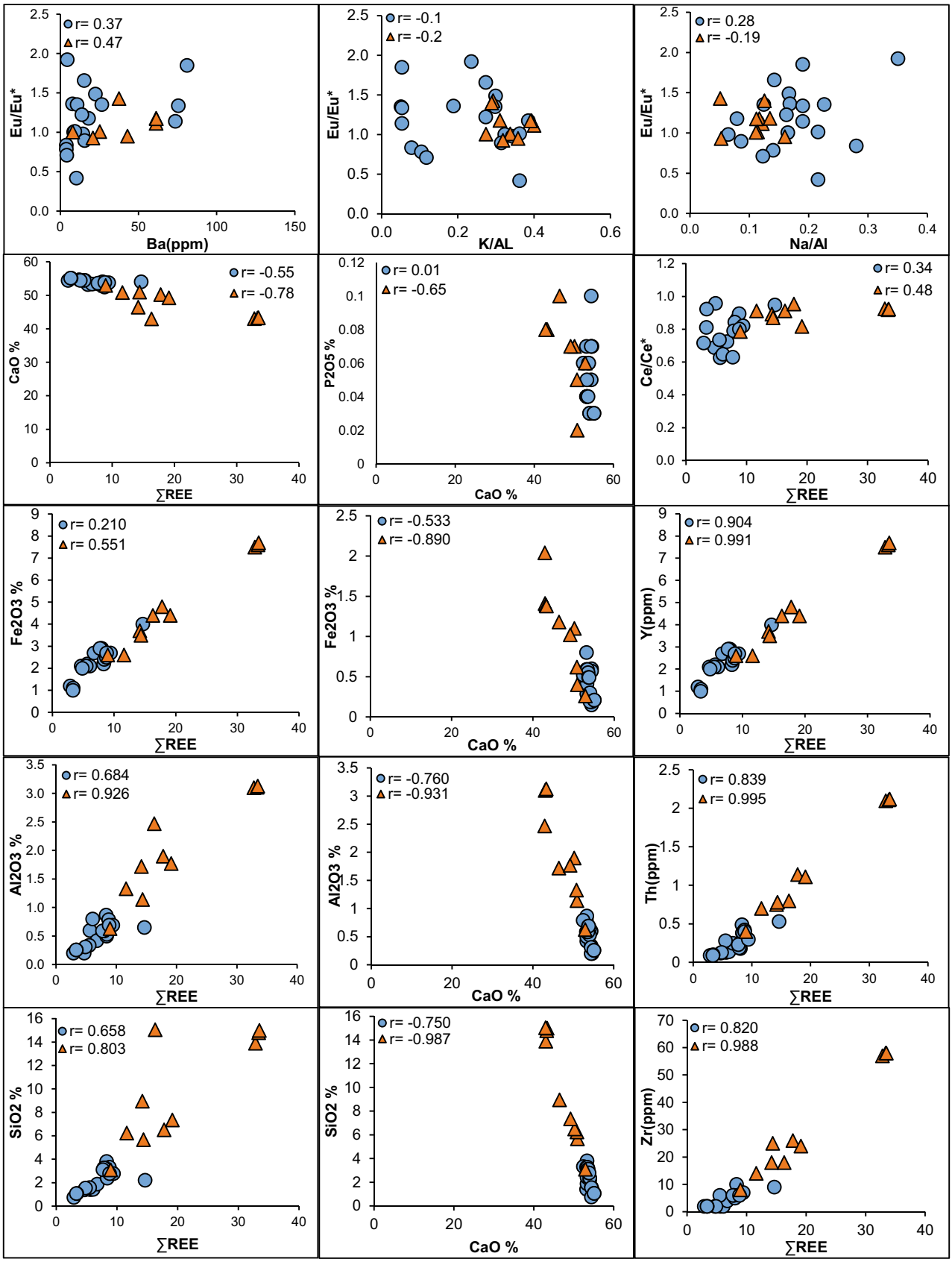

Fig. 5 Bivariate plots show the relationships of CaO% and ΣREE with some major oxides and trace elements and Eu/Eu* relations with K/Al and Na/Al ratios for the limestones of the Govanda Formation (blue circle = MSL, orange triangle = ML)

Table 2 Trace elements concentrations (ppm) for the carbonates from the Govanda Formation, Northeastern Iraq

		Large ion lithophile elements				High-field strength elements						Transitional trace elements						
Rocks	Samples	Ba	Rb	Cs	Sr	Th	U	Y	Zr	Hf	Nb	Sc	V	Cr	Co	Ni	Cu	Zn
Massive Limestone (MSL)	Sh2	3.8	0.4	0.01	362	0.12	4.42	2.1	2	0.1	0.1	2	25	240	1	12	8	8
	Sh3	3.9	0.8	0.02	351	0.13	4.43	2.2	2	0.1	0.1	2	27	230	1	13	7	10
	Sh4	4.1	1.5	0.09	342	0.14	4.44	2.1	2	0.5	0.1	3	27	210	2	11	9	11
	Sh8	22.5	2.5	0.17	519	0.25	2.42	2.7	4	0.1	0.3	2	9	20	1	12	4	12
	Sh11	4.5	1	0.05	430	0.09	3.81	1.2	2	0.1	0.2	2	15	20	1	6	2	34
	Sh13	8.5	1.5	0.08	620	0.28	3.4	2.1	6	0.2	0.3	2	12	40	1	9	4	203
	Sh14	7.8	1.9	0.13	440	0.38	3.63	2.3	7	0.2	0.4	2	19	50	1	10	3	73
	BS2	14.4	6.8	0.51	439	0.49	1.14	2.2	10	0.2	0.5	2	8	40	1	11	2	9
	BS3	15.6	4.9	0.32	346	0.53	0.76	4	9	0.1	0.5	2	12	40	1	11	6	7
	BS4	18	4.2	0.27	332	0.39	1.03	2.4	6	0.1	0.4	2	11	40	1	7	17	4
	HG1	10.8	0.9	0.02	327	0.13	2.39	2	2	0.1	0.1	2	13	70	1	25	3	3
	HG2	26.5	4.9	0.27	334	0.42	3.89	2.5	6	0.1	0.6	2	17	40	2	26	4	7
	HG3	73.6	0.9	0.05	304	0.18	1.56	2.9	5	0.1	0.3	2	17	990	3	39	3	6
	HG4	75.5	1.1	0.15	310	0.19	1.57	2.9	6	0.1	0.3	2	17	960	3	38	3	6
	HG5	81.1	1.3	0.17	312	0.23	1.6	2.9	6	0.1	0.4	2	17	900	4	38	4	7
	SG1	15.3	2.5	0.31	300	0.3	4.2	2.7	7	0.1	0.4	2	16	80	1	22	4	5
	SG2	13	2	0.27	304	0.4	4.32	2	6	1.1	1	4.3	16	70	1	0.5	4	6
	SG3	9.3	2	0.13	516	0.1	1.46	2	2	0.4	1	1.6	9	30	1	0.1	2	2
	SG4	10.3	2	0.12	521	0.09	1.62	2	2	0.6	1	1.7	10	30	1	0.1	2	3
	Average	22.07	2.35	0.17	389.95	0.25	2.74	2.32	4.84	0.14	0.30	2.05	15.63	215.79	1.47	18.32	4.79	21.89
Marly Limestone (ML)	Sh5	61.2	18	1.1	320	2.1	5.7	7.5	57	1.4	2.9	2	29	136	2	34	5	20
	Sh6	61.3	19.4	1.11	324	2.11	5.8	7.6	58	1.5	3.1	4	30	138	4	37	6	22
	Sh7	61.4	19.6	1.12	325	2.12	5.93	7.7	58	1.5	3.1	4	31	140	4	39	7	22
	Sh9	25.3	9.4	0.59	460	0.75	1.86	3.7	18	0.5	1.3	4	22	160	4	76	7	11
	Sh10	37.6	13	0.88	273	0.8	1.62	4.4	18	0.5	1.5	6	35	210	6	157	6	21
	Sh12	7.9	2.8	0.17	446	0.4	3.41	2.6	8	0.2	0.6	2	17	50	1	9	3	84
	Sh15	42.9	7.9	0.45	402	0.78	1.8	3.5	25	0.6	1.1	2	16	50	1	9	4	33
	BS1	20.9	9.8	0.71	377	0.7	1.12	2.6	14	0.3	0.8	3	11	40	1	20	3	15
	HA1	106	11.5	0.66	400	1.14	2.58	4.8	26	0.4	1.3	2	26	99	1	40	4	19
	HA2	120	12.5	0.72	419	1.11	2.54	4.4	24	0.4	1.3	2	24	110	1	42	4	19
	Average	54.45	12.39	0.75	374.60	1.20	3.24	4.88	30.60	0.73	1.70	3.10	24.10	113.00	2.50	46.30	4.90	26.60
	PAAS	650	160	15	200	14.6	3.1	27	210	5	19	16	150	110	23	55	50	85

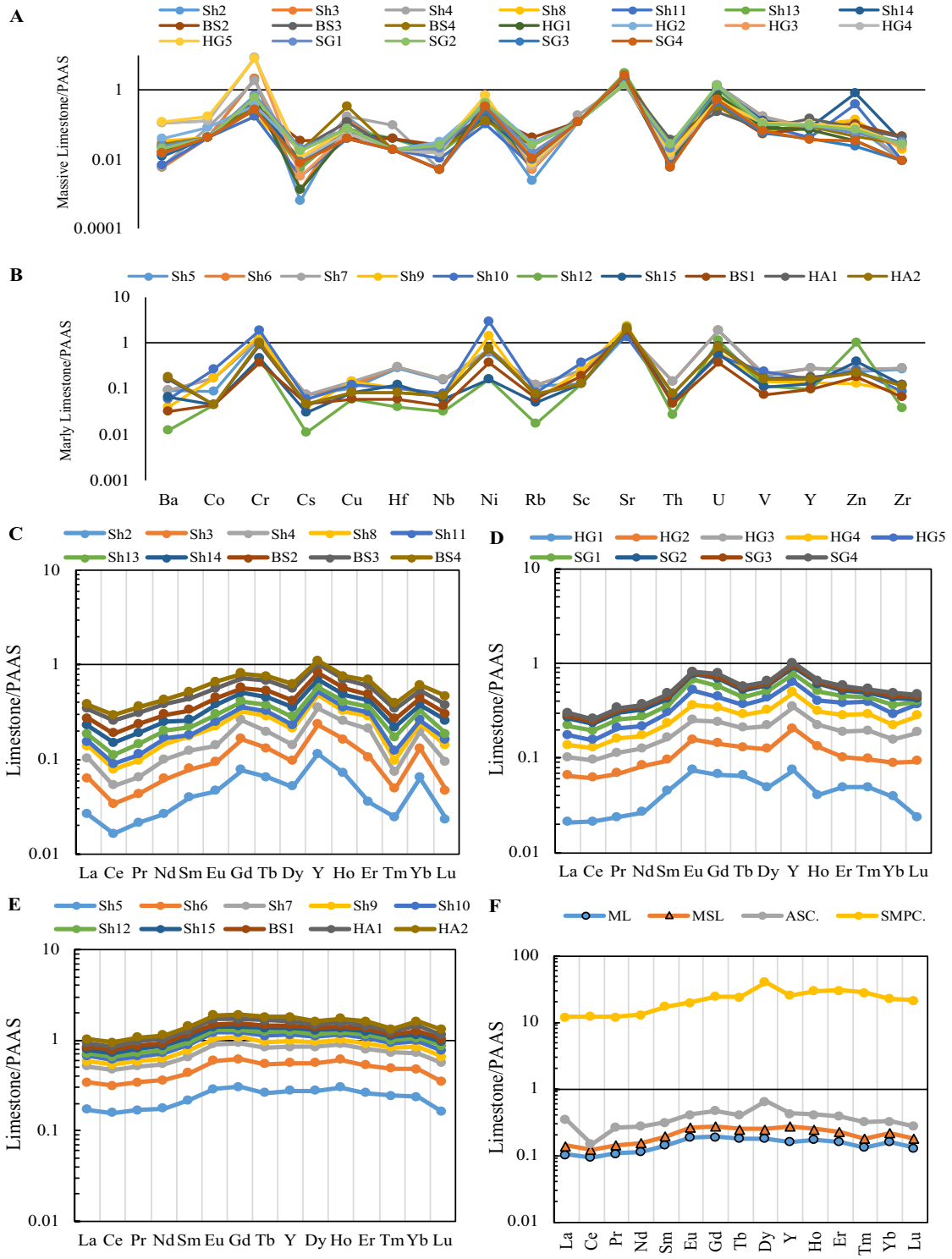

Fig. 6 Post-Archean Australian Shale (PAAS) normalized Major and trace elements: **A**, **C** and **D** = Massive limestone; **B**, and E Marly limestone, F PAAS-normalized comparison of average MSL and ML values, *ASC* Arabian Sea Carbonate sediments (Nath et al. 1997), SMPC shallow marine Carbonate platform (Mazumdar, 2003)

Table 3 Rare-earth element concentrations (in ppm) for the carbonates of the Govanda Formation, Northeastern Iraq

Rocks	S. No	La	Ce	Pr	Nd	Sm	Eu	Gd	Tb	Dy	Ho	Er	Tm	Yb	Lu	∑REE
Massive Limestone (MSL)	Sh2	1	1.3	0.19	0.9	0.22	0.05	0.36	0.05	0.24	0.07	0.1	0.01	0.18	0.01	4.68
	Sh3	1.4	1.4	0.19	1.2	0.22	0.05	0.41	0.05	0.21	0.09	0.2	0.01	0.19	0.01	5.63
	Sh4	1.5	1.5	0.19	1.3	0.25	0.05	0.44	0.05	0.21	0.09	0.3	0.01	0.18	0.02	6.09
	Sh8	1.4	2	0.29	1.6	0.28	0.09	0.29	0.07	0.32	0.07	0.21	0.01	0.12	0.02	6.77
	Sh11	0.6	0.9	0.14	0.7	0.03	0.03	0.18	0.03	0.1	0.03	0.08	0.01	0.06	0.01	2.9
	Sh13	1.1	1.8	0.29	1.1	0.23	0.05	0.24	0.04	0.24	0.05	0.13	0.02	0.2	0.01	5.5
	Sh14	1.7	3	0.39	1.7	0.22	0.09	0.44	0.06	0.33	0.08	0.19	0.02	0.14	0.03	8.39
	BS2	1.7	3	0.42	1.6	0.39	0.07	0.29	0.06	0.31	0.08	0.17	0.02	0.19	0.02	8.32
	BS3	2.7	5.4	0.64	2.9	0.65	0.13	0.72	0.11	0.62	0.13	0.33	0.03	0.26	0.03	14.65
	BS4	1.5	3	0.43	1.6	0.39	0.1	0.41	0.06	0.36	0.06	0.25	0.02	0.2	0.04	8.42
	HG1	0.8	1.7	0.21	0.9	0.25	0.08	0.31	0.05	0.23	0.04	0.14	0.02	0.11	0.01	4.85
	HG2	1.7	3.2	0.4	1.9	0.28	0.09	0.35	0.05	0.35	0.09	0.15	0.02	0.14	0.03	8.75
	HG3	1.4	2.7	0.39	1.5	0.37	0.1	0.46	0.06	0.44	0.09	0.25	0.04	0.19	0.04	8.03
	HG4	1.3	2.5	0.41	1.5	0.38	0.12	0.47	0.06	0.48	0.09	0.27	0.04	0.19	0.04	7.85
	HG5	1.41	2.1	0.42	1.52	0.39	0.17	0.48	0.06	0.51	2.9	0.09	0.28	0.04	0.19	7.7
	SG1	1.8	3.2	0.45	1.9	0.35	0.16	0.59	0.06	0.39	0.1	0.19	0.02	0.2	0.01	9.42
	SG2	1.7	2.9	0.41	1.9	0.32	0.11	0.56	0.06	0.33	0.1	0.18	0.02	0.2	0.01	8.8
	SG3	0.6	1.2	0.15	0.8	0.15	0.03	0.13	0.02	0.12	0.02	0.08	0.01	0.06	0.01	3.38
	SG4	0.7	1.1	0.14	0.5	0.18	0.02	0.28	0.02	0.16	0.03	0.11	0.01	0.08	0.01	3.34
	Ave	1.37	2.31	0.32	1.42	0.29	0.08	0.39	0.05	0.31	0.07	0.19	0.02	0.16	0.02	7.02
Marly Limestone (ML)	Sh5	6.5	12.5	1.5	6	1.2	0.31	1.43	0.2	1.3	0.3	0.74	0.1	0.67	0.07	32.82
	Sh6	6.6	12.6	1.52	6.2	1.21	0.33	1.44	0.22	1.31	0.3	0.76	0.1	0.68	0.08	33.35
	Sh7	6.6	12.7	1.53	6.2	1.22	0.33	1.44	0.22	1.31	0.3	0.76	0.1	0.68	0.09	33.48
	Sh9	2.7	5	0.62	2.8	0.67	0.15	0.73	0.1	0.53	0.09	0.35	0.04	0.36	0.04	14.18
	Sh10	3.1	5.9	0.72	3.2	0.66	0.2	0.66	0.12	0.69	0.15	0.46	0.04	0.37	0.05	16.32
	Sh12	1.8	3.1	0.46	1.8	0.37	0.08	0.38	0.09	0.31	0.07	0.22	0.03	0.22	0.04	8.97
	Sh15	2.6	5.3	0.76	3	0.63	0.12	0.56	0.1	0.58	0.1	0.27	0.04	0.28	0.04	14.38
	BS1	2.3	4.4	0.54	2	0.61	0.11	0.51	0.07	0.45	0.08	0.24	0.03	0.26	0.03	11.63
	HA1	3.1	6.9	0.9	3.6	0.54	0.2	0.84	0.15	0.4	0.16	0.32	0.03	0.6	0.05	17.79
	HA2	4.1	6.8	0.9	3.6	0.76	0.2	0.84	0.11	0.69	0.16	0.46	0.03	0.4	0.07	19.12
	Ave	3.94	7.52	0.95	3.84	0.79	0.2	0.88	0.14	0.76	0.17	0.46	0.05	0.45	0.06	20.2
	PAAS	38.2	79.6	8.83	33.9	5.55	1.08	4.66	0.77	4.68	0.99	2.85	0.41	2.82	0.43	184.7

Discussion

Source of the REE of the carbonates

The distribution pattern of REEs in limestones can be influenced by several factors, such as the addition of terrigenous materials from the continent (Piper 1974; McLennan 1989), scavenging process related to depth, salinity and oxygen levels (Elderfield 1988; Piepgras and Jacobsen 1992; Greaves et al. 1999), and diagenetic alterations which cause the REEs enrichments (Sholkovitz 1988). Therefore, clarifying the processes responsible for REE fractionation is essential since REEs are effective tracers of different geological and oceanographic processes (Piper 1974; Murray and Leinen 1993). The ΣREE content varies significantly between two types of limestone (MSL and ML) in all Govanda Formation sections, and they are less comparable with Arabian Sea carbonate sediments but relatively more or less comparable to shallow marine platform carbonate (78 ± 40, and 3.36 ± 2.55 ppm, respectively; Table 5) (Nath et al. 1997; Madhavaraju and Ramasamy 1999; Mazumdar et al. 2003). Significant positive correlation of ΣREE with SiO_2, Al_2O_3, Fe_2O_{3t}, Zr, Th, and Y and negative correlation with CaO% (Fig. 5), indicates that the source of REEs are impurities, including clays, ferruginous cement, quartz and heavy minerals like zircon.

The $(La/Yb)_n$ average value studied samples is similar to shallow marine platform carbonate ($(La/Yb)_n = 0.68 \pm 0.47$, Mazumdar et al. 2003). However, a few samples show values very close to that of the Arabian Sea carbonate sediments ($(La/Yb)_n = 0.85 \pm 0.2$, Nath et al. 1997; Table 5) and less than the value proposed by Condie (1991) [$(La/Yb)_n = 1$] and Sholkovitz (1990) [$(La/Yb)_n = 1.3$] for terrigenous

Table 4 Rare-earth element ratios for the carbonates of the Govanda Formation, Northeastern Iraq

Rocks	S. No	LREE	HREE	Ce/Ce*	Eu/Eu*	Gd/Gd*	Pr/Pr*	La/La*	Y/Ho	(La/Yb)n	(Dy/Yb)n	Pr/Yb	Pr/Sm	Er/Nd	(Nd/Yb)n	Sm/Yb
Massive Limestone (MSL)	Sh2	4.02	0.66	0.69	0.84	1.37	1.00	1.85	44.29	0.41	0.80	0.34	0.54	0.11	0.42	0.62
	Sh3	4.87	0.76	0.63	0.78	1.55	0.81	4.61	35.56	0.54	0.67	0.32	0.54	0.17	0.53	0.59
	Sh4	5.23	0.86	0.65	0.71	1.62	0.75	5.80	34.44	0.62	0.70	0.34	0.48	0.23	0.60	0.71
	Sh8	5.95	0.82	0.72	1.49	0.80	0.91	2.30	52.86	0.86	1.61	0.77	0.65	0.13	1.11	1.19
	Sh11	2.58	0.32	0.72	1.92	1.39	0.99	1.68	33.33	0.74	1.00	0.75	2.93	0.11	0.97	0.25
	Sh13	4.81	0.69	0.74	1.00	1.06	1.19	0.86	34.00	0.41	0.72	0.46	0.79	0.12	0.46	0.58
	Sh14	7.54	0.85	0.85	1.36	1.45	1.01	1.30	41.25	0.90	1.42	0.89	1.11	0.11	1.01	0.80
	BS2	7.47	0.85	0.82	0.98	0.83	1.12	0.92	40.00	0.66	0.98	0.71	0.68	0.11	0.70	1.04
	BS3	13.14	1.51	0.95	0.89	1.15	0.95	1.36	38.46	0.77	1.44	0.79	0.62	0.11	0.93	1.27
	BS4	7.43	0.99	0.86	1.18	1.17	1.15	0.76	40.00	0.55	1.08	0.69	0.69	0.16	0.67	0.99
	HG1	4.25	0.60	0.96	1.35	1.14	0.99	1.10	50.00	0.54	1.26	0.61	0.53	0.16	0.68	1.15
	HG2	7.92	0.83	0.90	1.35	1.25	0.94	1.50	38.89	0.90	1.51	0.91	0.90	0.08	1.13	1.02
	HG3	6.92	1.11	0.84	1.14	1.33	1.13	0.83	43.33	0.54	1.40	0.66	0.66	0.17	0.66	0.99
	HG4	6.68	1.17	0.79	1.34	1.35	1.23	0.67	43.33	0.51	1.52	0.69	0.68	0.18	0.66	1.02
	HG5	6.49	1.21	0.63	1.85	1.37	1.34	0.69	43.33	0.55	1.62	0.71	0.68	0.18	0.67	1.04
	SG1	8.45	0.97	0.82	1.66	1.73	1.06	1.12	37.00	0.66	1.18	0.72	0.81	0.10	0.79	0.89
	SG2	7.90	0.90	0.80	1.22	1.69	1.00	1.40	37.00	0.63	0.99	0.65	0.81	0.09	0.79	0.81
	SG3	3.06	0.32	0.92	1.01	1.06	0.88	1.78	55.00	0.74	1.21	0.80	0.63	0.10	1.11	1.27
	SG4	2.92	0.42	0.81	0.42	2.14	1.11	1.00	46.67	0.65	1.21	0.56	0.49	0.22	0.52	1.14
	Average	6.19	0.83	0.79	1.18	1.34	1.03	1.66	41.51	0.64	1.17	0.65	0.80	0.14	0.76	0.91
Marly Limestone (ML)	Sh5	29.44	3.38	0.92	1.11	1.13	1.02	1.09	25.00	0.72	1.17	0.71	0.79	0.12	0.74	0.91
	Sh6	29.90	3.45	0.92	1.18	1.06	1.01	1.13	25.33	0.72	1.16	0.71	0.79	0.12	0.76	0.90
	Sh7	30.02	3.46	0.92	1.17	1.06	1.01	1.11	25.67	0.72	1.16	0.72	0.79	0.12	0.76	0.91
	Sh9	12.67	1.52	0.89	1.01	0.89	0.97	1.39	37.00	0.55	0.89	0.55	0.58	0.13	0.65	0.95
	Sh10	14.44	1.88	0.91	1.43	1.03	0.97	1.33	29.33	0.62	1.12	0.62	0.69	0.14	0.72	0.91
	Sh12	7.99	0.98	0.79	1.00	0.66	1.13	0.94	37.14	0.60	0.85	0.67	0.78	0.12	0.68	0.85
	Sh15	12.97	1.41	0.87	0.95	1.00	1.11	0.84	35.00	0.69	1.25	0.87	0.76	0.09	0.89	1.14
	BS1	10.47	1.16	0.91	0.93	0.99	1.07	0.92	32.50	0.65	1.04	0.66	0.56	0.12	0.64	1.19
	HA1	16.08	1.71	0.95	1.40	0.53	1.06	0.86	30.00	0.38	0.40	0.48	1.05	0.09	0.50	0.46
	HA2	17.20	1.92	0.82	1.18	1.05	1.06	1.14	27.50	0.76	1.04	0.72	0.74	0.13	0.75	0.97
	Average	18.12	2.09	0.89	1.14	0.94	1.04	1.08	30.45	0.64	1.01	0.67	0.75	0.12	0.71	0.92

Table 5 Average values of elemental ratios of the studied area compared to the values of shallow marine platform carbonate and Arabian Sea Carbonate sediments

Ratio	Govanda formationa		Sea water	Shallow marine platform carbonateb	Arabian Sea Carbonate sedimentsc
	Massive limestone	Marly limestone			
Ce/Ce*	0.63–0.96	0.79–0.95	< 0.1–0.4[d]	–	0.84 ± 0.06
	0.79	0.89			
(La/Yb)n	0.41–0.90	0.38—0.76	0.2–0.5[e]	0.68 ± 0.47	0.85 ± 0.2
	0.64	0.64			
Gd/Gd*	0.80–2.14	0.53–1.13	1.30–1.05[f]	1.01 ± 0.20	1.09 ± 0.04
	1.34	0.94			
(Nd/Yb)n	0.42–1.13	0.50–0.89	0.205–0.497[g]	0.65 ± 0.39	0.85 ± 0.17
	0.76	0.71			
(Dy/Yb)n	0.67–1.62	0.40–1.25	0.8–1.1[h]	1.10 ± 0.25	1.12 ± 0.11
	1.17	1.01			
Y/Ho	33.3–55	25–37.14	~ 44–74[i]	35.90 ± 13.25	34.14 ± 1.64
	41.5	30.45			
Er/Nd	0.08–0.23	0.09–0.14	0.27[j]	0.25 ± 0.17	0.11 ± 0.02
	0.14	0.12			
Eu/Eu*	0.42–1.92	0.93–1.43	–	–	1.15 ± 0.08
	1.18	1.14			
∑REE	2.90–14.65	8.97–33.48	–	3.36 ± 2.55	78 ± 40
	7.02	20.2			
CaCO3%	95.8 ± 1.3	83.04 ± 6.45			51 ± 22

Ce/Ce* = Ce/(La_n x Pr_n)$^{0.5}$, Eu/Eu* = Eu_n/(Sm_n *Gd_n)$^{0.5}$, Pr/Pr* = [Pr/(0.5Ce+0.5Nd)]$_n$, Gd/Gd* =[Gd/(0.33Sm+0.67Tb)]$_n$, La/La* = Lan/($3Pr_n$ − $2Nd_n$); Bau and Dulski (1996)

[a]Study area (n = 29)

[b]Mazumdar et al. (2003)

[c]Nath et al. (1997)

[d, e]Elderfield And Greaves (1982)

[f]De baar et al. (1985)

[g](50 m water depth samples) zhang and Nozaki (1996)

[h]Webb And Kamber (2000)

[i]Bau et al. (1996)

[j]de Baar et al. (1988)

particulate matter. In addition, the Dy/Yb ratio of the MSL: 1.17 and ML: 1.01 found in the studied samples are similar to the Dy/Yb ratio observed in the Shallow Marine Platform Carbonate, which is 1.10 ± 0.25 (Mazumdar et al. 2003), and the Arabian Sea carbonates ratio of 1.12 ± 0.11 (Nath et al. 1997; Table 5). This information suggests that these limestones retained their original seawater characters. Meanwhile, in normal seawater, the Er/Nd ratio is about 0.27 (De Baar et al. 1988) and limestones with high Er/Nd ratios effectively represent the seawater signature that marine carbonates retain. However, the addition of detrital material or the effect of the diagenesis process can result in the reduction of the Er/Nd value to below 0.1 (De Baar et al. 1988; German and Elderfield 1989; Bellanca et al. 1997; Nagarajan et al. 2011). The Er/Nd ratios of the carbonates of the Govanda Formation range from 0.08 to 0.23 in the MSL and from 0.09 to 0.14 in the ML. This supports the pristine character of most samples, but some limestone samples exhibit values closer to 0.10, comparable to Arabian Sea carbonates (Nath et al. 1997; Table 5), indicating the influence of detrital material.

The Y/Ho ratio is a useful proxy for identifying the presence or absence of siliciclastic components in carbonate samples (Bau 1991; Özyurt et al. 2020). Uncontaminated marine carbonates by terrigenous material exhibit Y/Ho ratios that vary widely between ~ 44 and 74 or approximate the chondritic value of ~ 28 (Liu et al. 2019; Özyurt M. et al. 2020). In the present study, variations in Y/Ho ratios were observed among different types of limestone Govanda Formation (Table 4). The Y/Ho ratio in chemical sediments decreases as Nd increases, approaching the Y/Ho ratios observed in schists, which also have high Nd content. This implies a significant alteration of the REY budget by detrital aluminosilicates (Viehmann et al. 2015). The Y/Ho vs. Nd

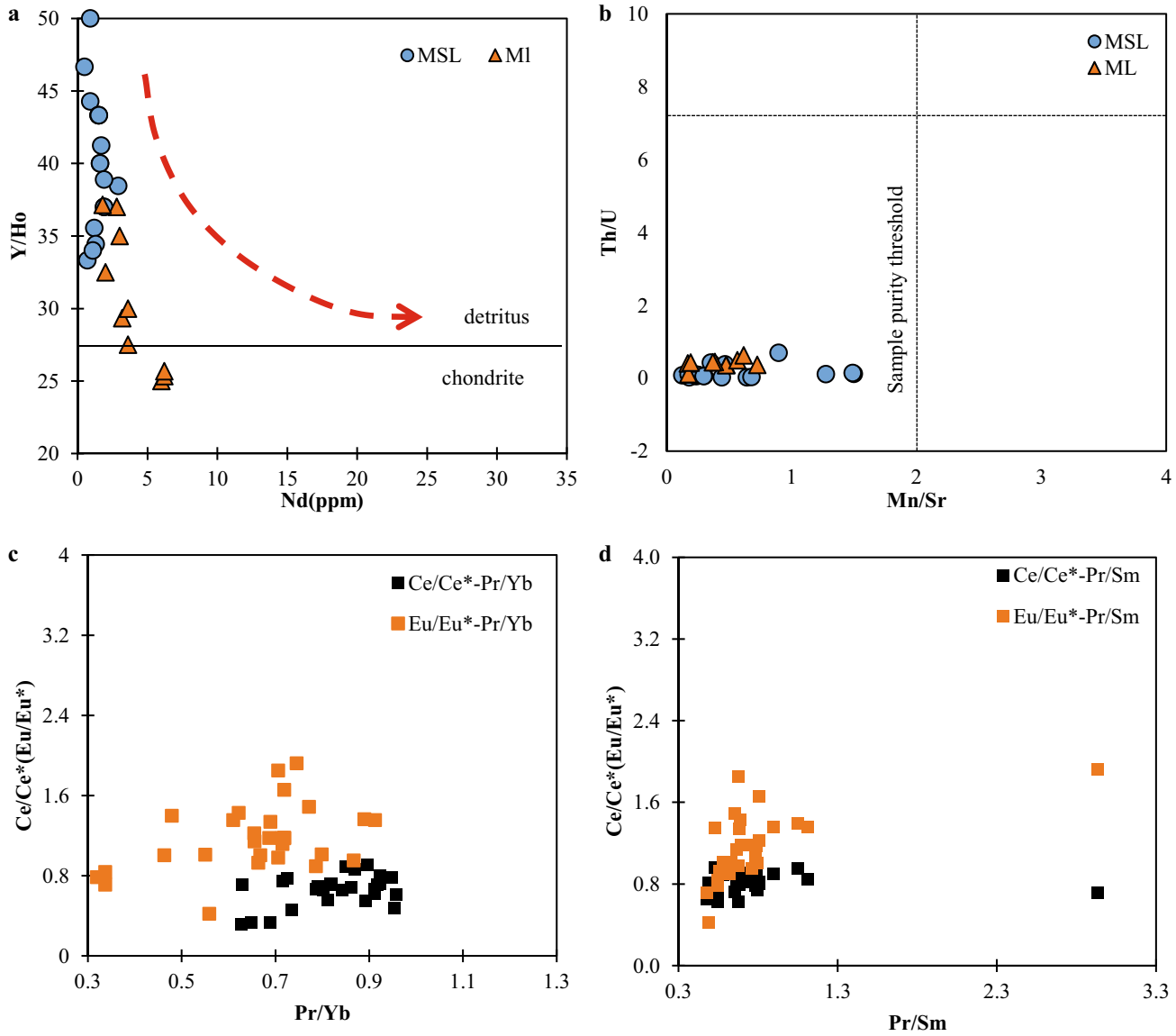

Fig. 7 **a** = Y/Ho vs. Nd concentration for the Govanda carbonates (Mishra and Mohanty 2021; detritus and chondrite trends are adopted from Viehmann et al. 2015). **b** Correlation diagram of Th/U vs. Mn/Sr ratios (after Li et al. 2022). **c**, **d** Evaluation of REEs anomaly to discriminate the alteration of Govanda Formation Samples. (After Li et al. 2022)

diagram of the studied carbonate shows a low concentration of Nd suggesting that the samples lean more toward pure chemical precipitates with the presence of some detrital contaminants (Fig. 7a).

The carbonate rock units of the Govanda Formation were deposited in an intermontane basin, flanked by positive lands, and show little or no negative Eu anomaly (Table 4) this might have been derived from the weathering of diverse lithologies during deposition. Some elemental ratios such as K/Al and Na/Al, are helpful for determining the presence of detrital feldspar in bulk sediments (Madhavaraju and Lee 2009). However, in the present study, K/Al and Na/Al ratios do not show any correlation with Eu/Eu* (Fig. 5), this suggests that the observed positive Eu anomaly in these limestones may not be due to the inclusion of feldspars. As well, the hydrothermal alteration probably did not contribute to positive Eu anomalies since LREE is depleted relative to HREE. According to Bau (1991); Wang et al. (2018) and Mishra and Mohanty (2021), the positive europium anomalies in studied carbonates can be attributed to the reducing environment of deposition.

Evaluation of diagenetic alteration

Hydrothermal alteration and burial metamorphic can occur during the early and late stages of diagenesis, leading to

the destruction of the original depositional information in carbonate rocks (Knauth and Kennedy, 2009; Li et al. 2022). The findings of our chemical analyses of major oxides in the present study revealed that calcite is the main mineral component of limestones of the Govanda Formation, which is consistent with the average content of CaO (51.6%). In addition, these limestones have a low Mg content, with an average of MgO values are: 1.16% in MSL and 1.39% in ML, indicating that little or a lack of dolomitization processes. Some geochemical parameters such as Mn/Sr ratios can be effectively used to evaluate the diagenetic alteration of carbonate rock (Kaufman et al. 1993; Wu, 2013). As the Mn content of precipitation is higher than that of seawater, the diagenetic alteration will be exhibited as an increase in the Mn/Sr ratio, therefore, the Mn/Sr ratio < 2 is considered to suggest that carbonate rock has not been affected by water interaction (Kaufman et al. 1993; Kaufman and Knoll 1995). The bivariate diagram between Mn/Sr and Th/U ratios can also reveal whether trace elements contain information relevant to the original deposition. Figure 7b illustrates a weak association between the Th/U ratio and Mn/Sr, suggesting that Th and U likely retain a record of the sedimentary information from ancient seawater. All limestone samples were characterized by Mn/Sr values of < 2 (Table 6) indicating that these limestones were not affected by diagenesis. REEs patterns in carbonate rocks are not affected by alteration or strong weathering (Webb and Kamber 2000). However, the behavior of certain elements, such as Ce and Eu, may vary due to differences in valence states under different redox conditions, leading to anomalies in their behavior and differentiation in rare earth element associations (Webb and Kamber 2000; Tribovillard et al. 2006; Li et al. 2022). According to Webb and Kamber (2000), in this study, we assessed the correlations between Ce/Ce*; Eu/Eu* and Pr/Yb; Pr/Sm as

Table 6 Major and trace elements ratios for the carbonates of the studied area

Rocks	Sample	Mn/Sr	Th/U	Ni/Co	Cr/V	V(V + Ni)	U/Th	Authigenic U	Sr/Ba	Sr/Rb
Massive Limestone (MSL)	Sh2	0.64	0.03	12.00	9.60	0.68	36.83	4.38	95.26	905.0
	Sh3	0.44	0.03	13.00	8.52	0.68	34.08	4.39	90.00	438.8
	Sh4	0.68	0.03	5.50	7.78	0.71	31.71	4.39	83.41	228.0
	Sh8	0.15	0.10	12.00	2.22	0.43	9.68	2.34	23.07	207.6
	Sh11	0.18	0.02	6.00	1.33	0.71	42.33	3.78	95.56	430.0
	Sh13	0.12	0.08	9.00	3.33	0.57	12.14	3.31	72.94	413.3
	Sh14	0.18	0.10	10.00	2.63	0.66	9.55	3.50	56.41	231.6
	BS2	0.35	0.43	11.00	5.00	0.42	2.33	0.98	30.49	64.6
	BS3	0.90	0.70	11.00	3.33	0.52	1.43	0.58	22.18	70.6
	BS4	0.47	0.38	7.00	3.64	0.61	2.64	0.90	18.44	79.0
	HG1	0.24	0.05	25.00	5.38	0.34	18.38	2.35	30.28	363.3
	HG2	0.23	0.11	13.00	2.35	0.40	9.26	3.75	12.60	68.2
	HG3	1.27	0.12	13.00	58.24	0.30	8.67	1.50	4.13	337.8
	HG4	1.50	0.12	12.67	56.47	0.31	8.26	1.51	4.11	281.8
	HG5	1.49	0.14	9.50	52.94	0.31	6.96	1.52	3.85	240.0
	SG1	0.26	0.07	22.00	5.00	0.42	14.00	4.10	19.61	120.0
	SG2	0.25	0.09	24.00	4.38	0.40	10.80	4.19	22.03	70.7
	SG3	0.30	0.07	15.00	3.33	0.38	14.60	1.43	55.48	322.5
	SG4	0.30	0.06	19.00	3.00	0.34	18.00	1.59	50.58	306.5
	Average	0.52	0.14	13.14	12.55	0.48	15.35	2.66	41.60	272.6
Marly Limestone (ML)	Sh5	0.73	0.37	17.00	4.69	0.46	2.71	5.00	5.23	17.8
	Sh6	0.48	0.36	9.25	4.60	0.45	2.75	5.10	5.29	16.7
	Sh7	0.48	0.36	9.75	4.52	0.44	2.80	5.22	5.29	16.6
	Sh9	0.17	0.40	19.00	7.27	0.22	2.48	1.61	18.18	48.9
	Sh10	0.57	0.49	26.17	6.00	0.18	2.03	1.35	7.26	21.0
	Sh12	0.17	0.12	9.00	2.94	0.65	8.53	3.28	56.46	159.3
	Sh15	0.19	0.43	9.00	3.13	0.64	2.31	1.54	9.37	50.9
	BS1	0.62	0.63	20.00	3.64	0.35	1.60	0.89	18.04	38.5
	HA1	0.39	0.44	40.00	3.81	0.39	2.26	2.20	3.77	34.8
	HA2	0.37	0.44	42.00	4.58	0.36	2.29	2.17	3.49	33.5
	Average	0.42	0.40	20.12	4.52	0.42	2.97	2.84	13.24	43.8

indicators of diagenetic alteration for all limestone samples of the Govanda Formation (PAAS-normalizing data). Except for the weak correlation between Ce/Ce* and Pr/Sm, the parameters (Ce/Ce*, Eu/Eu*, Pr/Yb, and Pr/Sm) showed a moderate linear relationship (with correlation coefficients of 0.60, 0.55 and 0.57) (Fig. 7c, d), indicating that the analyzed samples had not undergone diagenetic alterations.

Paleo-environmental analysis of the carbonates

The microfacies analysis revealed that the carbonates under investigation were formed in the shallow marine reef-fore-reef environment. This conclusion was drawn by combining the findings from petrography, and field studies and comparing them to standard facies models.

The enrichment of certain trace elements in marine sediments and their solubility in seawaters are influenced by oxygen levels, which determine their oxidation states (Hua et al. 2013; Tobia and Aqrawi 2016). For instance, uranium ions maintain a higher oxidation state (U^{+6}) in seawater but when trapped in marine carbonates change to a lower oxidation state (U^{+4}). On the other hand, thorium remains unaffected by the redox conditions of the water column and can persist indefinitely in its insoluble state of Th. (Hua et al. 2013). The use of authigenic U calculation can further support interpretations of the oxidative depositional condition using the following formula: authigenic U = Total U – (Th/3), the values of oxic conditions are indicated by < 2, whereas values exceeding 2 indicate dysoxic conditions (Wignall and Myers 1988). The results of the authigenic U calculations for the MSL and ML samples range from 0.58 to 4.39 (ave. = 2.66); and 0.88 to 5.22 (ave. = 2.84), respectively Table 6). These results suggest the limestones deposited in dyoxic conditions environment.

For evaluation of paleo-redox conditions, the trace element ratio indices, V/Cr, U/Th, Ni/Co, and V/(V + Ni), are used widely (e.g., Hatch and Leventhal 1992; Rimmer, 2004). According to Mishra and Mohanty (2021), the boundary of the Ni/Co ratio is at 3 for suboxic-anoxic and at 2 for dysoxic to oxic conditions. The V/(V + Ni) ratio is considered an anoxic condition of > 0.5, and suboxic to the oxic boundary at 0.3, while in oxic water the V/(V + Ni) ratio is < 0.5. We have employed the limited values of the U/Th ratio, which was suggested by Wignall and Richard (1996), to define the boundaries of the oxic conditions: oxic to suboxic is set at 0.1, the dysoxic limit ranges between 0.1 and 0.5, and the dysoxic to anoxic occurs at 0.5. According to the geochemical ratios, the studied carbonates were possibly deposited under suboxic–anoxic conditions within shallow water environments (Fig. 8).

The Ce* anomaly in carbonates is a more reliable proxy for determining ancient seawater redox state (Azmy et al. 2011; Liu et al. 2019; Özyurt et al. 2020). The depletion of Ce* anomalies represent modern oxygenated seawater (Bau 1991; Liu et al. 2019; Özyurt et al. 2020). However, it is important to mention that the partial leaching of clays containing high levels of REE + Y can mask any Ce anomalies present within the authigenic carbonate phase. Suboxic seawater mobilizes Ce-containing sediments, releasing Ce into the water column and creating a less negative to positive Ce anomaly in seawater (De Baar 1991). A significant negative Ce* anomaly can be categorized into three types: (a) smaller than < 0.5; (b) ~ 0.6–0.9; and (c) ~ 0.9–1.0, representing oxic, suboxic, and anoxic marine water, respectively (Chen et al. 2015; Özyurt et al., 2022). The negative Ce anomalies observed in this study (MSL: 0.63 to 0.96; ML: 0.79 to 0.95; Table 4) suggest that these limestones were deposited under a suboxic/anoxic environment, but the difference in Ce anomalies in these limestones indicates fluctuations of oxygen levels in the water which are close to those in Arabian sea sediments (Nath et al. 1997; Table 5).

Tectonic setting of Govanda Formation carbonates

Various studies have demonstrated that there were different tectonic settings for the deposition of Limestone successions, including continental margin basins (Wilson 1975), oceanic floors above the carbonate compensation depth (Liu and Schmitt 1990; Wang et al. 1986; Nath et al. 1997), local inland freshwater lakes (Alonso-Zarza 2003), and oceanic highs (Zhang et al. 2014). In general, limestones contain trace elements that originate from terrigenous materials and are scavenged from seawater (Murray et al. 1991; Siby et al. 2008). Numerous studies have demonstrated that the quantity and types of these terrigenous and trace elements in seawater are generally influenced by the plate tectonic environment of the basins (Murray et al. 1991; Holser 1997). Post-depositional alterations can modify the primary textures of limestones. Consequently, the relationship between the geochemistry and plate tectonics setting of limestones provides additional information for understanding ancient plate tectonic environments from the current variations in seawater chemistry (Webb and Kamber 2000). The Sr content of limestones found inland is lower than limestones in the open ocean, which exhibit the lowest Rb concentrations and the lowest Ba concentrations in limestones found along the continental margins (Zhang et al. 2017). The Rb–Sr–Ba ternary diagram to explain the studied samples reveals most of the samples fall within the marginal field (Fig. 9a). Furthermore, limestones from the continental margin can be distinguished from those from inland freshwater sources by their high Sr/Ba and Sr/Rb ratios in the Sr/Ba vs. Sr/Rb diagram. (Fig. 9b). Open-ocean limestones are mostly influenced by hydrothermal Fe–Mn-oxyhydroxide flux, while the inland and margin limestones are mostly influenced by terrigenous materials (Zhang et al. 2017). Al_2O_3 contents display

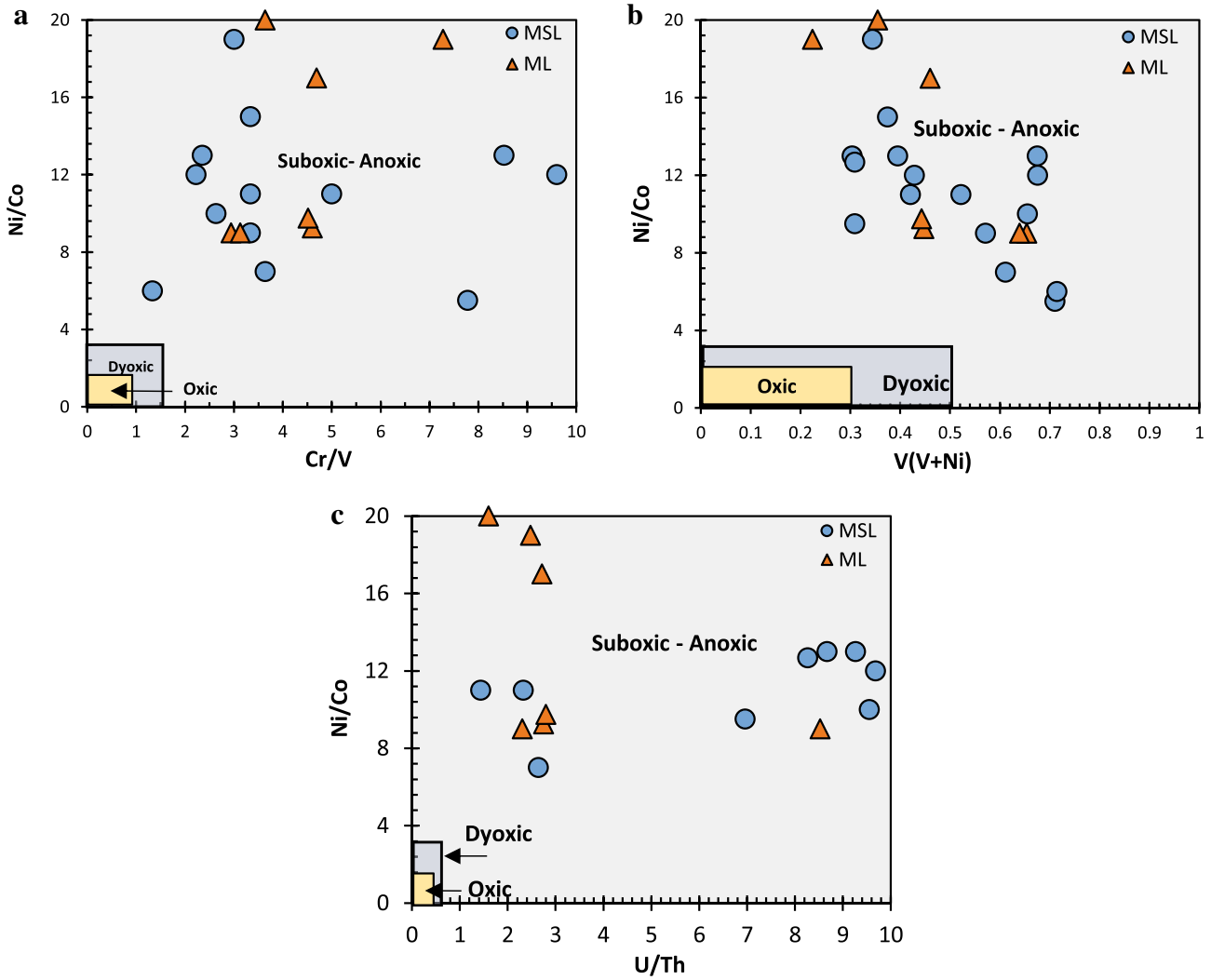

Fig. 8 Cross-plots of geochemical data of Govanda carbonates for assessing paleo-redox conditions: **a** Cr/V vs. Ni/Co; **b** V/(V + Ni) vs. Ni/Co; **c** U/Th vs. Ni/Co (Mishra and Mohanty 2021)

a positive correlation with Fe_2O_3 for the marine limestones (Fig. 9c), but these two variables are invariant for the inland limestones. According to the variation trend of the Ce/Ce* ratios and the proximity of the basin to a continental plate margin, the limestones can be classified into two groups: inland + margins vs. open ocean (Zhang et al. 2017). Figure 9d reveals the limestones of the studied area represent the passive margin tectonic setting, which is less affected by terrigenous materials.

Conclusions

1. Depending on the content of Al_2O_3% and SiO_2% and the purity of limestones, the Middle-Miocene Govanda Formation was subdivided into massive limestone (MSL) and marly limestone (ML), composed predominantly of calcite.
2. The total rare earth element (∑REE) content in the limestones of the Govanda Formation is lower compared to the Arabian Sea carbonate sediments. Light rare earth element depletion (LREE) and enrichment of heavy rare earth element (HREE) and (La/Yb)n ratio in the limestone samples indicate that the seawater REE pattern was preserved despite the presence of a degree of detrital contamination that affected the REE content and element ratios of these samples.
3. The limestone beds have a consistent seawater-like REE pattern, indicating the retention of seawater characteristics in the limestones, slightly negative Ce anomalies (Ce/Ce* = 0.79 in MSL and = 0.89 in ML), relatively positive Eu anomalies (Eu/Eu* = 1.18 in MSL and = 1.14 in ML), and Y/Ho ratios are moderately high (37.69). The REE + Y pattern of samples mainly retains its original characters, but the positive correlation of

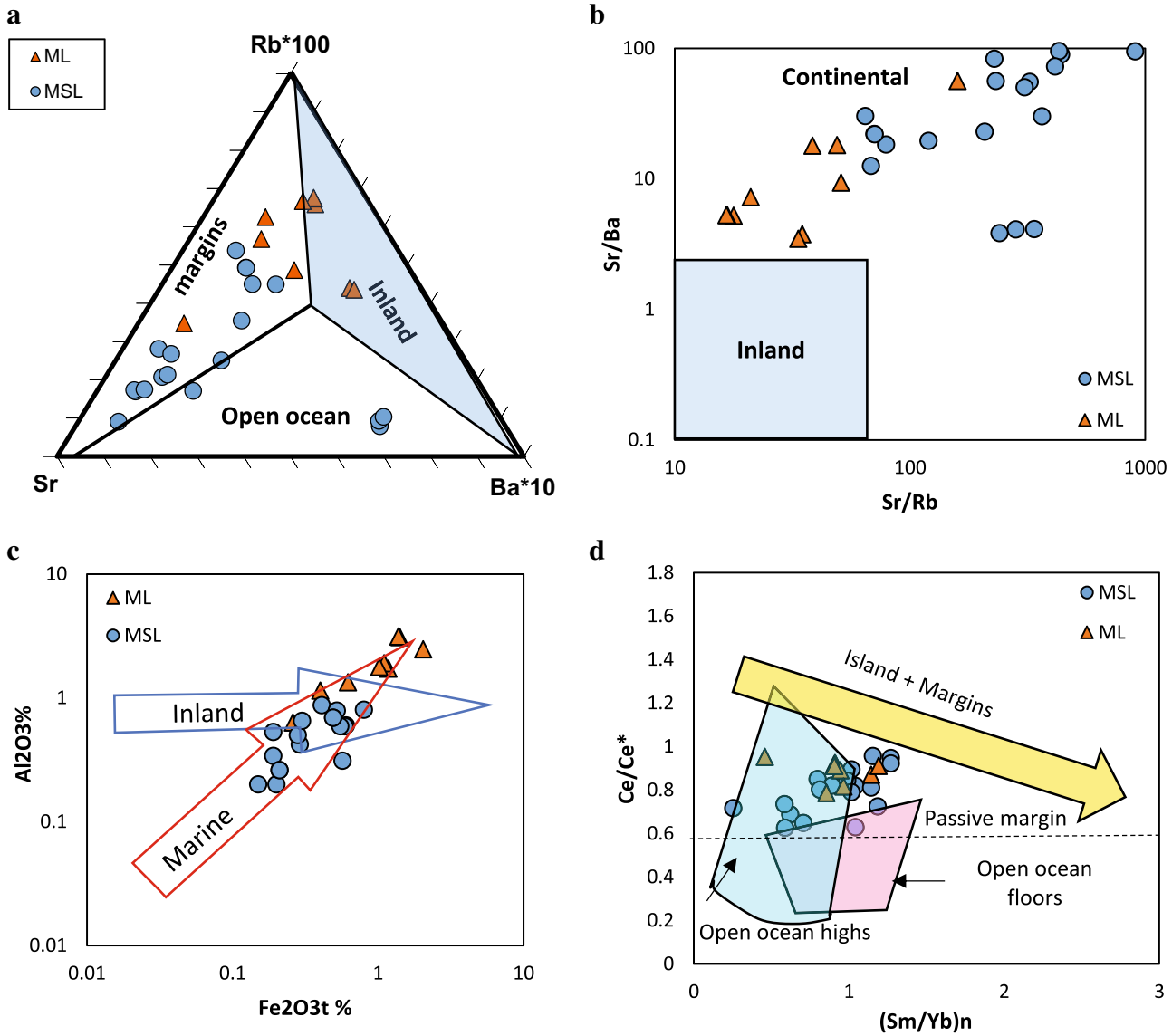

Fig. 9 **a** Rb–Sr–Ba triangular diagram, **b** Sr/Ba vs. Sr/Rb, **c** Al2O3% vs. Fe2O3%, and **d** Ce/Ce* vs. Sm/Yb bivariate analyses represent the passive margin tectonic setting which is less affected by terrigenous materials (after Zhang et al. 2017)

ΣREE with Th, Zr, and Y confirms the detrital inputs source of REEs.

4. The Y/Ho vs. Nd diagram of the studied carbonate shows a low concentration of Nd suggesting that the samples lean more toward pure chemical precipitates.
5. The weak association of Mn/Sr with Th/U ratios and Mn/Sr values of < 2 indicates that these limestones were not affected by diagenetic alterations.
6. Authigenic U, trace element indices (V/Cr, U/Th, Ni/Co, and V/(V + Ni)), and negative Ce anomalies reveal the suboxic to anoxic conditions of deposition.
7. The microfacies revealed a shallow marine reef-fore-reef environment for the Govanda carbonates.
8. Al_2O_3% contents display a positive correlation with Fe_2O_3% and are mostly related to marine limestones rather than inland limestones. The Rb–Sr-Ba ternary diagram, and Sr/Ba vs. Sr/Rb, Al_2O_3% vs. Fe_2O_3%, and Ce/Ce* vs. Sm/Yb bivariate analyses imply that the studied limestones originated in the passive margin tectonic setting.

Acknowledgements We express our gratitude to Dr. Azad T. Saeed and Prof. Dr. Sardar M. Balaky (Soran University) for their assistance during fieldwork. We extend our appreciation to Prof. Dr. Yawooz A. Kettanah (Dalhousie University) for his invaluable scientific guidance and discussion. We would also like to acknowledge the anonymous reviewers for their helpful comments.

Author contributions Research methodology, data collecting, data analysis, and interpretation of results were all conducted by Zh S Abdulrehman. Fieldwork, data collecting, and methodology were all supervised by Assistant Professor A M Aqrawi. Review, correction, and helpful suggestions for improvement were all offered by Dr. R I Koshnaw and Asst. Prof. A M Aqrawi.

Funding The authors did not receive support from any organization for the submitted work.

Data availability Data available on request from the authors.

Declarations

Conflict of interest The authors declare that there are no competing interests.

References

Abdula RA, Chicho J, Surdashy A, Nourmohammadi MS, Hamad E, Muhammad MM, Smail AA, Ashoor A (2018) Sedimentology of the Govanda Formation at Gali Baza locality. Kurdistan Region, Iraq: Iraqi Bull of Geol Mining 14(1):1–12

Allen MB, Armstrong HA (2008) Arabia-Eurasia collision and the forcing of mid-Cenozoic global cooling. Palaeogeo Palaeoclim Palaeoeco 265(1–2):52–58

Armstrong-Altrin JS, Verma SP, Madhavaraju J, Lee YI, Ramasamy S (2003) Geochemistry of Late Miocene Kudankulam Limestones, South India. Intern Geol Rev 45:16–26

Azmy K, Brand U, Sylvester P, Gleeson SA, Logan A, Bitner MA (2011) Biogenic and abiogenic low-Mg calcite (bLMC and aLMC): Evaluation of seawater-REE composition, water masses, and carbonate diagenesis. Chem Geol 280:180–190

Bau M (1991) Rare-earth element mobility during hydrothermal and metamorphic fluid-rock interaction and the significance of the oxidation state of europium. Cheml Geol 93:219–230

Bau M, Koschinsky A, Dulski P, Hein JR (1996) Comparison of the partitioning behaviors of yittrium, rare earth elements, and titanium between hydrogenetic marine ferromanganese crusts and seawater. Geochim Et Cosmochim Acta 60:1709–1725

Bellanca A, Masetti D, Neri R (1997) Rare earth elements in limestone/marlstone couplets from the Albian-Cenomanian Cismon section (Venetian region, northern Italy): assessing REE sensitivity to environmental changes. Chem Geol 141(3–4):141–152

Buday T, (1980) The Regional Geology of Iraq, Vol 1: Stratigraphy and Paleogeography. Publications of Geological Survey of Iraq, Baghdad: 445

Caetano-Filho S, Paula-Santos GM, Dias-Brito D (2018) Carbonate REE + Y signatures from the restricted early marine phase of South Atlantic Ocean (late Aptian–Albian): the influence of early anoxic diagenesis on shale-normalized REE + Y patterns of ancient carbonate rocks. Paleogeo Palaeoclim Palaeoeco 500:69–83

Chen J, Algeo TJ, Zhao L, Chen ZQ, Cao L, Zhang L, Li Y (2015) Diagenetic uptake of rare earth elements by bioapatite, with an example from Lower Triassic conodonts of South China. Earth-Sci Rev 149:181–202. https://doi.org/10.1016/j.earscirev.2015.01.013

Condie KC (1991) Another look at rare earth elements in shales. Geochim Et Cosmochim Acta 55:2527–2531

De Baar HJ (1991) On cerium anomalies in the Sargasso Sea. Geochim Et Cosmochim Acta 55:2981–2983

De Baar HJ, Bacon MP, Brewer PG (1985) Rare earth elements in the Pacific and Atlantic oceans. Geochim Et Cosmochim Acta 49:1943–1959

De Baar HJ, German CR, Elderfield H, Van Gaans P (1988) Rare earth element distributions in anoxic waters of the Cariaco Trench. Geochim Et Cosmochim Acta 52:1203–1219

Dunham RJ (1962) Classification of carbonate rocks according to depositional textures. AAPG Mem 1:108–121

Elderfield H (1988) The oceanic chemistry of the rare earth elements. Philos Trans R Soc Lond 325:105–126

Elderfield H, Greaves MJ (1982) The rare earth elements in seawater. Nature 296:214–219

Elderfield H, Upstill-Goddard R, Sholkovitz ER (1990) The rare earth elements in rivers, estuaries and coastal seas and their significance to the composition of ocean waters: Geochim. et Cosmochim. Acta 54:971–991

German CR, Elderfield H (1989) Rare earth elements in Saanich Inlet, British Columbia, a seasonally anoxic basin. Geochim Et Cosmochim Acta 53:2561–2571

Greaves MJ, Elderfield H, Sholkovitz ER (1999) Aeolian sources of rare earth elements to the Western Pacific Ocean. Mari Chem 68:31–38. https://doi.org/10.1016/S0304-4203(99)00063-8

Haldar SK, (2000) Introduction to Mineralogy and Petrology. (2nd ed), The Min Geol and Metal Inst (MGMI) Kolkata, West Bengal, India, The Indian Geological Congress (IGC).

Hempton MR (1987) Constraints on Arabian plate motion and extensional history of the Red Sea. Tectonics 6(6):687–705. https://doi.org/10.1029/TC006i006p00687

Jassim SZ, Buday T, Cichea I, Prouza V (2006) Late Permian-Liassic Megasequence AP6. In: JASSIM, S.Z., GOFF, J. (eds) Regional geology of Iraq. Dolin, Prague and Moravian Museum, Brno: 104–116.

Kaufman AJ, Knoll AH (1995) Neoproterozoic variations in the C isotopic composition of seawater; stratigraphic and biogeochemical implications. Precam Rese 73:27–49

Kaufman AJ, Jacobsen SB, Knoll AH (1993) The Vendian record of Sr and C isotopic variations in seawater: Implications for tectonics and paleoclimate. Earth Planetary Sci Lett 120:409–430

Koshnaw RI, Stockli DF, Schlunegger F (2019) Timing of the Arabia-Eurasia continental collision—Evidence from detrital zircon U-Pb geochronology of the Red Bed Series strata of the northwest Zagros hinterland. Kurdistan Region of Iraq Geology 47(1):47–50. https://doi.org/10.1130/G45499.1

Koshnaw IR, Horton KB, Stockli DF, Barber DE, Tamar-Agha MY (2020) Sediment routing in the Zagros foreland basin: drainage reorganization and a shift from axial to transverse sediment dispersal in the Kurdistan region of Iraq. Basin Res 32(4):688–715. https://doi.org/10.1111/bre.12391

Koshnaw RI, Schlunegger F, Stockli DF (2021) Detrital zircon provenance record of the Zagros mountain building from the Neotethys obduction to the Arabia-Eurasia collision, NW Zagros fold–thrust belt. Kurdistan Region Iraq Solid Earth 12(11):2479–2501. https://doi.org/10.5194/se-12-2479-2021

Li J, Gui H, Chen L, Fang P, Li X, Zhang J, Wang Y (2022) Geochemistry of upper Palaeozoic 'thin-layer' limestones in the southern North China Craton: implications for closure of the northeastern Palaeotethys Ocean. Geol Mag 159:494–510. https://doi.org/10.1017/S0016756821001126

Liu XM, Hardisty DS, Lyons TW, Swart PK (2019) Evaluating the fidelity of the cerium paleoredox tracer during variable carbonate diagenesis on the great Bahamas Bank. Con Et Cosmochi Acta 248:25–42. https://doi.org/10.1016/j.gca.2018.12.028

Lokesh BP, (2015) Sedimentology provenance and depositional environments of Kurnool group palnad sub basin Andhra Pradesh South India. PhD. dissertation, University of Mysore, Karnataka, India

Madhavaraju J, Lee Y (2009) Geochemistry of the Dalmiapuram formation of the Uttatur Group (Early Cretaceous), Cauvery basin, southeastern India: implications on provenance and paleo-redox conditions. Rev Mexic De Cienc Geol 26:380–394

Madhavaraju J, Ramasamy S (1999) Rare earth elements in limestones of Kallakurichchi Formation of Ariyalur Group, Tiruchirappalli Cretaceous, Tamil Nadu. J of Geol Soci of India 54:291–301

Madhavaraju J, González-León CM, Lee YI, Armstrong-Altrin JS, Reyes-Campero LM (2010) Geochemistry of the mural formation (Aptian-Albian) of the Bisbee group, Northern Sonora. Mexico Cretac Res 31:400–414

Madhavaraju J, Ramírez-Montoya E, Monreal R, González-León CM et al (2016) Paleoclimate, paleoweathering and paleoredox conditions of Lower Cretaceous shales from the Mural Limestone, Tuape section, northern Sonora, Mexico: constraints from clay mineralogy and geochemistry. Revi Mexic De Cienci Geoló 33(1):34–48

Mazumdar A, Tanaka K, Takahashi T, Kawabe I (2003) Characteristics of rare earth element abundances in shallow marine continental platform carbonates of Late Neoproterozoic successions from India. Geochem J 37:277–289

Mclennan SM, (1989). Rare earth elements in sedimentary rocks; influence of provenance and sedimentary processes. In: Lipin BR, McKay GA (eds.), Geochemistry and Mineralogy of Rare Earth Elements. Revi in Min, 21: 169–200

Miller KG, Browning JV, Schmelz WJ, Kopp RE, Mountain GS, Wright JD (2020) Cenozoic sea-level and cryospheric evolution from deep-sea geochemical and continental margin records. Adv, Sci. https://doi.org/10.1126/sciadv.aaz1346

Mishra PK, Mohanty SP (2021) Geochemistry of carbonate rocks of the Chilpi Group, Bastar Craton, India: Implications on ocean paleoredox conditions at the late Paleoproterozoic Era. Precam Resea 353:106023

Mohammadkhani H, Hosseini-Barzi M, Sadeghi A, Pomar L (2022) Middle Miocene short-lived Tethyan seaway through the Zagros foreland basin: facies analysis and paleoenvironmental reconstruction of mixed siliciclastic- carbonate deposits of Mishan Formation, Dezful Embayment. SW Iran Marine Petroleum Geology 140:105649. https://doi.org/10.1016/j.marpetgeo.2022.105649

Murray RW, Leinen M (1993) Chemical transport to the seafloor of the equatorial Pacific Ocean across a Latitudinal transect at 135 °W. Tracking sedimentary major, trace and rare earth element fluxes at the Equator and the Intertropical Convergence Zone. Geochim Cosmochim Acta 57:4141–4163

Murray RW, Brink MRB, Brumsack HJ, Gerlach DC, Russ GP III (1991) Rare earth elements in Japan Sea sediments and diagenetic behavior of Ce/Ce∗: results from ODP Leg 127. Geochim Cosmochim Acta 55:2453–2466

Nagarajan R, Madhavaraju J, Armstron-Altrin JS, Nagendra R (2011) Geochemistry of Neoproterozoic limestones of the Shahabad formation, Bhima Basin, Karnataka, Southern India. Geos J 15:9–25

Nath BN, Bau M, Ramalingeswara RB, Rao CM (1997) Trace and rare earth elemental variation in Arabian Sea sediments through a transect across the oxygen minimum zone. Geochim Cosmochim Acta 61:2375–2388

Özyurt M, Kirmaci MZ, Al-Aasm I, Hollis C, Tasli K, Kandemir R (2020) REE Characteristics of lower cretaceous limestone succession in Gümü¸ shane, NE Turkey: implications for ocean paleoredox conditions and diagenetic alteration. Minerals 10(683):510

Piepgras DJ, Jacobsen SB (1992) The behaviours of rare earth elements in seawater: Precise determination of ferromanganese crusts. Geochim Et Cosmochim Acta 56:1851–1862

Piper DZ (1974) Rare earth elements in the sedimentary cycle, a summary. Chem Geol 14:285–304

Sholkovitz ER (1988) Rare earth elements in the sediments of the North Atlantic ocean, Amazon delta, and east China Sea: reinterpretation of terrigenous input patterns to the oceans. Ameri J of Scie 288:236–281

Sholkovitz ER (1990) Rare earth elements in marine sediments and geochemical standards. Chem Geol 88:333–347

Sissakian VK, Fouad SF (2014) Geological Map of Sulaimaniyah Quadrangle, scale 1: 250 000, 2nd ed., Iraq Geological Survey (GEOSURV) Publications, Baghdad, Iraq.

Smail AA (2015) Sedimentology and stratigraphy of Govanda Formation, Unpublished MSc. University of Salahadin, Thesis, p 156

Taylor SR, Mclennan SM (1985) The continental crust: its composition and evolution. Blackwell Scientific Publications, Oxford, p 312

Tobia FH, Aqrawi AM (2016) Geochemistry of rare earth elements in carbonate rocks of the Mirga Mir Formation (Lower Triassic), Kurdistan Region. Iraq Arab J of Geos 9:259

Van Bellen RC, (1959) Stratigraphic Lexicon of Iraq: Lexique Stratigraphique International, Asie (Iraq). III, Asie Fascicule 10a, Iraq, Tertiary/by RC van Bellen, Mesozoic and Palaeozoic/ by Dunnington HV, Wetzel R, Morton DM, Centre National de la Recherche Scientifique, Paris, DL.

Veizer J, (1983) Chemical diagenesis of carbonates: theory and application of trace element technique. In: Stable Isotopes in Sedimentary Geology. ed. by Arthur, M. A., Anderson, T. F., Kaplan, I. R., Veizer, J. and Land, L. S. SEPM Short Course, 10. SEPM, Dallas, 3.1–3.100.

Viehmann S, Bau M, Hoffmann JE, Münker C (2015) Geochemistry of the Krivoy Rog banded Iron Formation, Ukraine, and the impact of peak episodes of increased global magmatic activity on the trace element composition of Precambrian seawater. Preca Resea 270:165–180

Wang YL, Liu Y-G, Schmitt RA (1986) Rare earth element geochemistry of South Atlantic deep sea sediments: Ce anomaly change at~ 54 My. Geochim Cosmochim Acta 50:1337–1355

Wang W, Bolhar R, Zhou M, Zhao X (2018) Enhanced terrestrial input into Paleoproterozoic to Mesoproterozoic carbonates in the southwestern South China block during the fragmentation of the Columbia supercontinent. Preca Resea 313:1–17

Webb GE, Kamber BS (2000) Rare earth elements in Holocene reefal microbialites: a new shallow seawater proxy. Geochim Cosmochim Acta 64:1557–1565

Wignall PB, Myers KJ (1988) Interpreting the benthic oxygen levels in mud rocks, a new approach. Geology 16(5):452–455

Zachos J, Pagani M, Sloan L, Thomas E, Billups K (2001) Trends, rhythms, and aberrations in global climate 65 Ma to present. Science 292:686–693

Zadeh PG, Adabi MH, Hisada KI, Hosseini-Barzi M, Sadeghi A, Ghassemi MR (2017) Revised version of the Cenozoic collision along the Zagros orogen: Insights from Cr-spinel and sandstone modal analyses. Scientific Report 7:10828. https://doi.org/10.1038/s41598-017-11042-1

Zhang J, Nozaki Y (1996) Rare earth elements and yttrium in seawater: ICP-MS determinations in the East Caroline, Coral Sea, and South Fiji basins of the western South Pacific Ocean. Geochim Et Cosmochim Acta 60:4631–4644

Zhang K-J, Xia B, Zhang Y-X, Liu W-L, Zeng L, Li J-F, Xu L-F (2014) Central Tibetan Meso-Tethyan oceanic plateau. Lithos 210:278–288

Zhang K-J, Li Q-H, Yan L-L, Zeng L, Lu L, Zhang Y-X, Hui J, Jin X, Tang X-C (2017) Geochemistry of limestones deposited in various plate tectonic settings. Earth Sci Rev 167:27–46